FEBRUARY 2024

M.Sc. in Materials Science and Engineering

BILAL MANSOUR

REPUBLIC OF TÜRKİYE

GAZİANTEP UNIVERSITY

GRADUATE SCHOOL OF NATURAL & APPLIED SCIENCES

MANGANESE BASED ELECTRODES IN ALKALINE AND NEUTRAL ELECTROLYTES FOR FLEXIBLE ENERGY STORAGE DEVICES

M.Sc. THESIS

IN

MATERIALS SCIENCE AND ENGINEERING

BY

BILAL MANSOUR

FEBRUARY 2024

MANGANESE BASED ELECTRODES IN ALKALINE AND NEUTRAL ELECTROLYTES FOR FLEXIBLE ENERGY STORAGE DEVICES

M.Sc. Thesis

in

Materials Science and Engineering

Gaziantep University

Supervisor

Asst. Prof. Dr. Abdulcabbar YAVUZ

by

Bilal MANSOUR

February 2024

I hereby declare that all information in this document has been obtained and presented in accordance with academic rules and ethical conduct. I also declare that, as required by these rules and conduct, I have fully cited and referenced all material and results that are not original to this work.

Bilal MANSOUR

ABSTRACT

MANGANESE BASED ELECTRODES IN ALKALINE AND NEUTRAL ELECTROLYTES FOR FLEXIBLE ENERGY STORAGE DEVICES

MANSOUR, Bilal
M.Sc.Thesis in Materials Sceince And Engineering
Supervisor: Assoc. Prof. Dr. Abdulcabbar YAVUZ
February 2024
60 pages

Flexible electrodes have been researched for e-textile. Screens have been produced as flexible and commercially are available. However, flexible energy storage and conversion devices have not been produced and commercialised. The motivation of this study is to fabricate flexible electrodes for energy storage and conversion devices. The research focuses on the electrodeposition of manganese onto graphite substrates using deep eutectic solvents (DESs). The study aims to optimize electrode conditions (growth and cycling) to achieve electrodes with high electrochemical stability, extensive active surface coverage, and enhanced areal capacitance. The experimental approach involves the preparation of electrode from Ethaline solutions having $MnCl_2$ by applying various potentials (-1.5 V, -2.0 V, and -2.5 V) for 500 seconds. The electrodes are then characterized using techniques such as X-ray diffraction (XRD), Fourier transform infrared spectroscopy (FTIR), and scanning electron microscopy (SEM). Electrochemical properties are assessed through cyclic voltammetry in 1 M KOH and 1 M Na_2SO_4 electrolytes for fuel cell and supercapacitor applications. The resulting coatings were not suitable for hydrogen evolution in alkaline electrolyte. The findings reveal that lower deposition potentials (more negative voltage) lead to a denser manganese layer and higher potentials (less negative potential) could cause thinner film. The thinner films resulted in higher specific capacitance and electrochemical performance because ions could have high flux on coating. The study contributes to the field of energy storage devices by demonstrating the potential of manganese-coated graphite electrodes in alkaline and neutral media for flexible supercapacitor applications, offering a promising alternative to expensive materials.

Key Words: Energy Storage; Supercapacitor; Alkaline Solution; Manganese; Flexible Graphite; Electrode; Characterization.

ÖZET

ESNEK ENERJİ DEPOLAMA CİHAZLARI İÇİN ALKALİ VE NÖTR ELEKTROLİTLERDE MANGANEZ BAZLI ELEKTROTLAR

MANSOUR, Bilal
Yüksek Lisans Tezi, Malzeme Bilim ve Mühendisliği
Danışman: Doç. Prof. Dr. Abdulcabbar YAVUZ
Şubat 2024
60 sayfa

Esnek elektrotlar, e-tekstil için araştırılmıştır. Ekranlar esnek olarak üretilmiş ve ticari olarak mevcuttur. Ancak, esnek enerji depolama ve dönüştüme cihazları henüz üretilmemiş ve ticarileştirilmemiştir. Bu çalışmanın motivasyonu, enerji depolama ve dönüştürme cihazları için esnek elektrotlar üretmektir. Araştırma, derin ötektik çözeltiler (DESs) kullanarak grafit substratlara manganezin elektrokaplamasına odaklanmaktadır. Çalışma, yüksek elektrokimyasal stabiliteye, geniş aktif yüzey kaplamasına ve geliştirilmiş alan kapasitansına sahip elektrotlar elde etmek için elektrot koşullarını (büyüme ve döngüleme) optimize etmeyi amaçlamaktadır. Deneysel yaklaşım, $MnCl_2$ içeren Ethaline çözeltilerinden çeşitli potansiyeller (-1.5 V, -2.0 V ve -2.5 V) uygulanarak 500 saniye boyunca elektrotların hazırlanmasını içermektedir. Daha sonra elektrotlar, X-ışını kırınımı (XRD), Fourier dönüşümlü kızılötesi spektroskopisi (FTIR) ve taramalı elektron mikroskobu (SEM) gibi teknikler kullanılarak karakterize edildi. Elektrokimyasal özellikler, 1 M KOH ve 1 M Na_2SO_4 elektrolitlerindeki döngüsel voltametri ile yakıt hücresi ve süperkapasitör uygulamaları için değerlendirildi. Elde edilen kaplamalar alkali çözeltide hidrojen oluşturmak için uygun değildi. Bulgular, daha düşük kaplama potansiyellerinin (daha negatif voltaj) daha yoğun bir manganez katmanına yol açtığını ve daha yüksek potansiyellerin (daha az negatif potansiyel) daha ince bir film oluşturabileceğini ortaya koymaktadır. Daha ince filmler daha yüksek spesifik kapasiteye ve elektrokimyasal performansa sebep oldu çünkü kaplamadaki iyonlar daha yüksek akışa sahip olabilirler. Çalışma, manganez kaplı grafit elektrotların alkali ve nötr ortamlarda esnek süperkapasitör uygulamaları için potansiyelini göstererek, pahalı malzemelere alternatif vaat eden enerji depolama cihazları alanına katkıda bulunmaktadır.

Anahtar Kelimeler: Enerji Depolama; Süperkapasitör; Alkali Çözelti; Manganez; Esnek Grafit; Elektrot; Karakterizasyon.

"Dedicated to my family"

ACKNOWLEDGEMENTS

I would like to thank my supervisor, Assoc.Prof. Dr. Abdulcabbar YAVUZ for his guidance and support throughout the study. I am thankful for his encouragement and motivation.

I would like to express my love and gratitude to my family for their support, always best wishes.

TABLE OF CONTENTS

Page

ABSTRACT ..... **vi**
ÖZET ..... **v**
ACKNOWLEDGEMENTS ..... **viii**
TABLE OF CONTENTS ..... **ix**
LIST OF TABLES ..... **xi**
LIST OF FIGURES ..... **xii**
LIST OF SYMBOLS ..... **xiv**
LIST OFABBREVIATIONS ..... **xv**
CHAPTER 1 INTRODUCTION **1**
1.1 Motivation of the Study 1
1.2 Objectives and Scope of the Study 1
1.3 Structure of the Thesis 2
CHAPTER 2 LITERATURE REVIEW **4**
2.1 Energy Storage Systems 4
2.2 Fuel Cell 4
2.3 Batteries 5
2.4 Capacitors 6
2.5 Supercapacitors 6
2.5.1 Electric Double Layer Capacitors 7
2.5.2 Pseudocapacitors 9
2.5.3 Hybrid Supercapacitors 9
2.6 Electrodeposition 10
2.7 Supercapacitor Electrolytes 11
2.7.1 Conventional Electrolytes 11
2.7.2 Ionic Liquids 12
2.7.3 Deep Eutectic Solvents 12
2.8 Characterization of Supercapacitor Materials 13
2.8.1 X-Ray Diffraction (XRD) 13
2.8.2 Fourier Transform Infrared Spectroscopy (FTIR) 13
2.8.3 Scanning Electron Microscopy (SEM) 14

2.9 Electrochemical Analysis of Supercapacitors 14
2.9.1 Chronoamperometry 14
2.9.2 Chronocoulometry 15
2.9.3 Cyclic Voltammetry 15
CHAPTER 3 EXPERIMENTAL PROCEDURES 16
3.1 Used Devices, Tools, and Materials Preparation Materials 16
3.1.1 Chemicals in the Experiment 18
3.2 Preparation of Electrodes 18
3.3 Preparation of Deep Eutectic Solvent 20
3.4 Element Selection and Preparation for Electrode Modification 22
3.5 Preparation of Electrolytes 23
3.6 Study of Manganese-Coated Graphite Samples for Supercapacitor Electrodes with Electrochemical Characterization Techniques 23
3.6.1 Chronocoulometry Analysis 24
3.6.2 Chronoamperometry 24
3.6.3 Cyclic Voltammetry 25
3.7 Study of Manganese Coated on Graphite Sample Non-Electrochemical Characterization Techniques 26
3.7.1 X-Ray Diffractometer (XRD) Analysis 26
3.7.2 Scanning Electron Microscopy (SEM) 27
3.7.3 Fourier Transform Infrared Spectroscopy (FTIR) Analysis 27
CHAPTER 4 RESULTS AND DISCUSSION 28
4.1 Manganese Growth on Flexible Graphite 28
4.2 SEM Analysis of Flexible Electrodes 32
4.3 XRD Analysis of Flexible Electrodes 33
4.4 FTIR Analysis of Flexible Electrodes 36
4.5 Fuel Cell Application of The Electrodes 37
4.6 Cycling of Electrodes in Na_2SO_4 Electrolyte 38
4.7 Analysis of the Electrodes in Na_2SO_4 with Different Scan Rates 41
4.8 Cycling of Electrodes in KOH Electrolyte 43
4.9 Analysis of the Electrodes in KOH with Different Scan Rate 45
4.10 Comparation Specific Capacitance of Electrodes in KOH and Na_2SO_4 47
CHAPTER 5 CONCLUSION 50
REFERENCES 52
CURRICULUM VITAE 60

LIST OF TABLES

Page

Table 3.1 Catalogue of Laboratory Apparatus and Reagents Employed in the Experimental Investigations 17

Table 3.2 Chemicals Employed in Experimental Procedures 18

Table 4.1 Specific capacitance values of Mn coated graphite tapes obtained at -1.5 V potential depending on the varying scanning rates in different electrolyte solutions 47

Table 4.2 Specific capacitance values of Mn coated graphite tapes obtained at -2 V potential depending on the varying scanning rates in different electrolyte solutions 47

Table 4.3 Specific capacitance values of Mn coated graphite tapes obtained at -2.5 V potential depending on the varying scanning rates in different electrolyte solutions 48

LIST OF FIGURES

Page

Figure 2.1 Schematic of the Lithium-ion battery 6
Figure 2.2 Schematic representation of EDLC 8
Figure 2.3 Sketch definition of pseudocapacitors 9
Figure 2.4 Schematic illustrator of hybrid supercapacitor 10
Figure 2.5 Diagram of electrolytes typically utilized in supercapacitors..... 11
Figure 3.1 Photos of materials used in the experiments..... 16
Figure 3.2 Photos of working electrodes' preparation phases 20
Figure 3.3 Photos of Ethaline preparing steps 21
Figure 3.4 Photos illustrate preparing 1M $MnCl_2$ in Ethaline..... 22
Figure 3.5 Photos illustrate graphite tape coating 24
Figure 3.6 Photos of conducting Cyclic voltammetry Test..... 25
Figure 4.1 Cyclic voltammogram results of bare graphite in (black line) Ethaline having $MnCl_2$, (red line) pure Ethaline in Room Temperature and (blue 28
Figure 4.2 Chronoamperometry data for the electrode obtained by application of -1.5 V, -2 V and -2.5 V for transferring to a) Na_2SO_4 and; b) KOH. Chronocoulometry data for the electrode obtained by application of -1.5 V, -2 V and -2.5 V for transferring to c) Na_2SO_4 and; d) KOH. The growth of the Mn was conducted at 60^o C for 500 seconds..... 30
Figure 4.3 Photos of Bubbles Appeared During the Coating Process When Appling a)-2V; b)-2.5V and c) -2.5V..... 31
Figure 4.4 Photos of a) bare graphite and Mn coated graphite on tape from Ethaline Deep Eutectic Solvent by the application of b) -1.5 V; c) -2.0 V and; d) -2.5 V..... 31
Figure 4.5 SEM results for bare and Mn coated graphite tapes. The growth potentials of the film are given under each image. 34
Figure 4.6 XRD results of bare graphite and Mn coated graphite. The deposition potential of each electrode is presented in the panels. 35

Figure 4.7 FTIR results for bare and Mn coated graphite tapes. The growth potential of the electrode is shown in the panel. 37

Figure 4.8 Linear Sweep Voltammetry of Bare and Manganese-Coated Graphite in KOH to Evaluate Electrodes Properties for Fuel Cell with Scan Rate of 20 mV s^{-1} 38

Figure 4.9 Cyclic voltammogram data cycled in Na_2SO_4. The cycling electrodes were electrodeposited when the growth potential was -1.5 V and cycling potential window a) between -0.8 and 0.5 V; b) between -0.8 and 0.2 V. Cyclic voltammogram data cycled in Na_2SO_4. The cycling electrodes were electrodeposited when the growth potential was c) -2.0 V and; d) -2.5 V..... 40

Figure 4.10 a) Cyclic voltammogram data cycled in Na_2SO_4. The cycling electrodes were electrodeposited when the growth potential was a) -1.5 V b) -2.0 V and; c) -2.5 V. The scan rates are indicated in the panels.... 42

Figure 4.11 a) Cyclic voltammogram data cycled in KOH. The cycling electrodes were electrodeposited when the growth potential was a) -1.5 V b) -2.0 V and; c) -2.5 V. The scan rates are indicated in the panels. 44

Figure 4.12 a) Cyclic voltammogram data cycled in KOH. The cycling electrodes were electrodeposited when the growth potential was a) -1.5 V b) 2.0 V and; c) -2.5 V. The scan rates are indicated in the panels. 46

Figure 4.13 specific capacitance of the modified electrodes cycled in a) Na_2SO_4 and b) KOH electrolyte. 49

LIST OF SYMBOLS

Mn	Manganese
$MnCl_2$	Manganese Chloride
Na_2SO_4	Sodium Sulfate
KOH	Potassium Hydroxide
ChCl	Choline Chloride
EG	Ethylene Glycol
Pt	Platinum
V	Voltage
I, i	Current
M	Molarity
Å	Angstrom
Θ	Theta
°	Degree
C	Centigrade Celsius
C_s	Capacitance
q, Q	Charge

LIST OFABBREVIATIONS

EDLCs	electric double-layer capacitors
HER	Hydrogen evolution reaction
DES	Deep Eutectic Solvent
EDLC	Electric Double Layer Capacitor
XRD	X-Ray Diffraction
SEM	Scanning Electron Microscopy
FTIR	Fourier Transform Infrared Spectroscopy
CV	Cyclic Voltammogram
IL	Ionic Liquid

CHAPTER 1
INTRODUCTION

1.1 Motivation of the Study

The motivation for this study is focus on the urgent global shift towards more sustainable energy storage solutions. In this context, supercapacitors and fuel cells stand out as a key technology due to their superior performance (charge-discharge speed, longevity, and reliability compared to traditional batteries). A critical challenge in electrode development (for either a supercapacitor or fuel cell) lies in identifying cost-effective yet high-performing materials. This study is particularly interested in the application of deep eutectic solvents (DESs) as electrolytes in electrode fabrication. DESs have shown promise in creating electrodes that exhibit exceptional electrochemical stability, extensive active surface area, and enhanced electrical conductivity [1]. Additionally, the exploration of transition metal oxides for fuel cell and supercapacitor electrodes is a promising avenue, potentially offering a cost-effective alternative to traditional materials while maintaining high performance and durability [2] .

1.2 Objectives and Scope of the Study

This research aims to investigate and optimize the electrodeposition conditions of transition metal oxide electrodes for fuel cells and supercapacitors, focusing on their performance in alkaline media. The primary goal is to fabricate electrodes that demonstrate high stability and superior electrochemical performance using novel methods. In this regard, the utilization of non-aqueous ionic liquids, specifically DESs, for fabricating nanostructured electrodes is a groundbreaking approach in the field of electrode development [3]. The study encompasses the development of these electrodes on cost-efficient substrates, assessing their performance in terms of stability, usability, and durability over extended cycling in various electrolytes. A comprehensive non-electrochemical characterization of the electrodes, employing advanced techniques like FTIR, XRD, and SEM, is also a crucial part of this research,

providing insights into the structural and compositional aspects of the electrodes in different operational conditions[4].

1.3 Structure of the Thesis

Chapter I: Introduction

This chapter sets the stage for the thesis by introducing the subject of alloy catalysts for hydrogen evolution reaction in alkaline solution and electrodes for supercapacitors. It outlines the general purpose of the thesis, presents its hypothesis, and provides a summary of the structure of the entire thesis. This chapter aims to establish the context and significance of the research within the broader field of sustainable energy and electrocatalysis.

Chapter II: Literature Review

The second chapter delves into the theoretical background and literature related to the study. It discusses the basic concepts of hydrogen energy, the role of electrocatalysis in energy storage systems, and the significance of developing alternative electrodes for energy storage and conversion systems. This section also covers the history and working principles of different energy storage systems, comparing them with the focus of this study. Additionally, it briefly describes the non-electrochemical characterization techniques (XRD, FTIR, SEM) and electrochemical characterization techniques (chronocoulometry, chronoamperometry, cyclic voltammetry) used in this research.

Chapter III: Experimental Procedures

The third chapter provides a comprehensive description of the experimental procedures employed in the study. It details the experimental equipment and chemicals used and elaborates on how the experiments were conducted. This includes the preparation processes of base electrodes, coating solutions, electrolyte solutions (KOH and Na_2SO_4), and the specific methods used in the cyclic voltammetry studies of the alloy electrodes. The chapter also explains how the various characterization techniques were applied to each study, ensuring a thorough understanding of the experimental approach.

Chapter IV: Results and Discussion

In the fourth chapter, the findings obtained from the experimental studies are presented and discussed in depth. This chapter synthesizes the results, drawing effective inferences and conclusions. It examines the study's predictions, compares the results with existing literature, and evaluates the contributions of the thesis to the field of electrocatalysis and hydrogen energy. The discussion addresses the thesis's hypothesis and aims, supported by relevant graphs, figures, and tables.

CHAPTER 2
LITERATURE REVIEW

2.1 Energy Storage Systems

Energy Storage Systems represent a diverse array of methods and structures designed for conserving energy. This stored energy is later utilized for productive purposes. Many renewable energy sources, such as wind, solar, and tidal energy, are intermittent by nature. However, their output is significantly influenced by geographical and climatic factors[5]. There are occasions when renewable energy, despite being available, is not immediately utilized. In such scenarios, energy storage becomes essential, allowing for the use of energy as and when required. Energy can be stored in various forms, including radiation, chemical, electrical potential, electric current, elevated temperature, latent heat, and kinetic energy. The storage of energy can be achieved through a range of methods and technologies, categorized into electrochemical [6], [7] thermodynamic and mechanical [8] storage. The selection of a particular energy storage technology is typically based on the specific application, cost-effectiveness, and integration into existing systems. The choice of technology for energy storage is also influenced by the availability of resources, along with economic and application considerations. Energy storage devices play a critical role in transforming energy from forms that are complex to store into more accessible or economically viable formats.

2.2 Fuel Cell

A fuel cell is an electrochemical device, like batteries, that transforms chemical energy from a fuel like hydrogen into electrical energy. Hydrogen is delivered to the cathode, the positive electrode, while oxygen is sent to the anode, the negative electrode. An electric current is produced as the protons move through the electrolyte and the electrons move through an external circuit. Water is formed at the cathode when protons and electrons from the external circuit interact with the oxygen in the air. In the results, this generates electrical energy from a fuel cell.

As understood by our previous information, the definition of energy for us consumers' energy demanders is the form that is available for use wherever and whenever required. Achieving these criteria is possible with energy storage systems and technologies such as batteries, fuel cells, capacitors, supercapacitors, etc. Due to the various designs of such fundamental storage technologies that are still under development as batteries, fuel cells, capacitors, and supercapacitors as well as the variances in the storage concept, there exist discrepancies in attributes. It can be explained as high storage capacity, high charge/discharge efficiency (%), low self-discharge and capacity losses, long life, low cost, and energy-intensive (kWh/kg or kWh/liter) are characteristics that differ depending on the type of storage technology.

2.3 Batteries

The advancement of battery energy storage technology is key to the shift from fossil fuels to renewable energy sources [9]. As the availability of renewable energy and the demand for electricity both rise, the importance of battery storage technologies grows [10]. These technologies allow for the collection and timely delivery of renewable energy from sources like solar and wind to meet consumer needs. Lithium-ion batteries, commonly found in mobile phones, laptops, electric vehicles, and other applications, are a leading energy storage solution in larger buildings to ensure a steady supply of renewable energy[11].

Batteries, composed of multiple voltaic cells linked in series, generate a stable voltage. They store charge through redox reactions involving two electrodes and an electrolyte. The electrodes, known as the anode (negative terminal) and cathode (positive terminal), are submerged in an electrolyte, typically acidic or basic. In these reactions, one substance donates electrons and transfers ions to another. Larger electrodes provide greater current capacity, enabling batteries to store and dispense significant energy [12]. While batteries can store and deliver substantial energy, their major limitation is the duration required for charging and discharging. **Figure 2.1** depicts a diagram of a battery [13].

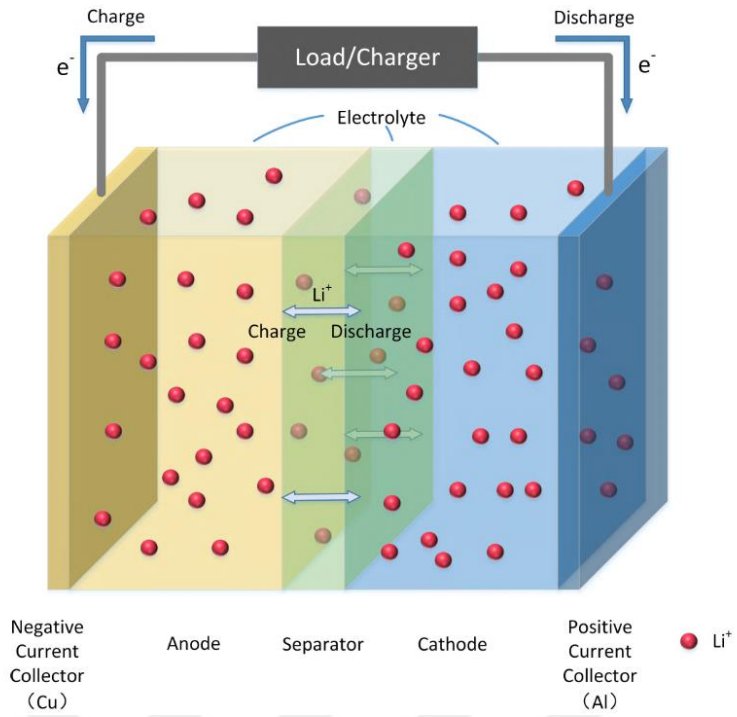

Figure 2.1 Schematic of the Lithium-ion battery [13]

2.4 Capacitors

When two parallel conductor plates are exposed to a voltage differential and separated by a dielectric material, one plate accumulates positive charges, while the opposite plate holds negative charges [14]. The amount of charge stored on these plates is directly proportional to the applied voltage, and the capacitor's capacitance is defined as the ratio of the stored charge to the voltage difference. This capacitance is influenced by three primary factors: the surface area of the plates, the distance between them, and the dielectric constant of the intervening material. To enhance capacitance, one can increase the plate surface area, decrease the distance between the plates, or modify the dielectric material. Modern supercapacitors feature large surface areas and thin dielectrics, effectively reducing the separation distance. The capacitance of a capacitor, denoted as C, is determined by measuring the charge (Q) on the plates relative to the voltage (V) across them, following the formula C = Q/V. The classic equation to compute the charge on the plates is given by Q = C x V.

2.5 Supercapacitors

Supercapacitors, alternatively known as ultracapacitors, are characterized by their significantly larger surface areas and reduced spacing between plates compared to

conventional capacitors. This difference is due to the unique function of their plate separators, which diverge from the standard dielectric role [15].

Prominent advantages of supercapacitors include their prolonged lifecycle, high operational efficiency, and the incorporation of environmentally sustainable components [16]. While 'supercapacitor' and 'ultracapacitor' terms are often used interchangeably, they differ in construction; they are made from distinct materials and assembled in varied configurations, resulting in different energy storage capacities.

Like a standard capacitor, a supercapacitor comprises two separate metal plates. These plates are coated with a porous substance such as powdered activated charcoal, significantly increasing the surface area for enhanced charge storage [17]. Analogous to the difference between a towel's limited absorption capacity and a sponge's extensive capacity, the porous plates in supercapacitors act as robust electricity absorbers.

In traditional capacitors, the plates are separated by a relatively thicker dielectric, which could be mica, a thin plastic film, or simply air. When charged, positive ions accumulate on one plate while negative ions gather on the other, generating an electric field. This field polarizes the dielectric, aligning its molecules in the reverse direction and subsequently decreasing the field's strength. This suggests that at a given voltage, the plates can hold a greater amount of charge.

Supercapacitors are categorized into three primary types: electric double-layer capacitors, hybrid capacitors, and pseudocapacitors. Each type exhibits unique properties and functions, contributing to the diversity of this energy storage technology.

2.5.1 Electric Double Layer Capacitors

Supercapacitors, also known as electric double-layer capacitors (EDLCs) or ultracapacitors, offer an advanced approach to power system quality and reliability in short-term applications. In EDLCs, electricity is stored within the electrical field created between isolated plates, much like in traditional capacitors. The capacitance here depends on the surface area of the plates, the space between them, and the dielectric properties of the separator [18]. The unique feature of EDLCs lies in the

dispersion of electric charges, which results from the directional orientation of electrochemical reactions at the electrode material/electrolyte interface [19].

In these systems, excess electrical charges accumulate on the electrode surfaces, while ions in the electrolyte, carrying opposite charges, gather in the surrounding medium [20]. During charging or discharging, positive ions in the electrolyte migrate towards the negatively charged electrode, and negative ions move towards the positive electrode, with electrons flowing from the negative to the positive electrode through the external circuit.

EDLCs, when paired with batteries in hybrid storage systems, provide an effective solution for managing the energy demands of off-grid photovoltaic (PV) systems. The EDLC caters to sudden spikes in energy demand, while the battery delivers steady power over extended periods. This design allows the battery to be sized for continuous loads rather than peak current demands, which are significantly higher but last for shorter durations. The EDLC's ability to handle substantial energy fluctuations and prevent deep battery discharges extends the battery's lifespan [21].

In hybrid storage systems featuring EDLCs and batteries, the batteries experience reduced discharge rates, resulting in prolonged battery life and the need for lighter batteries. This hybrid structure enhances the durability of the photovoltaic system both in the short and long term. High power quality in the system ensures that fluctuations in load demands do not adversely affect the standalone system, making off-grid photovoltaic solutions more feasible in previously challenging environments. **Figure 2.2** illustrates a schematic representation of an EDLC.

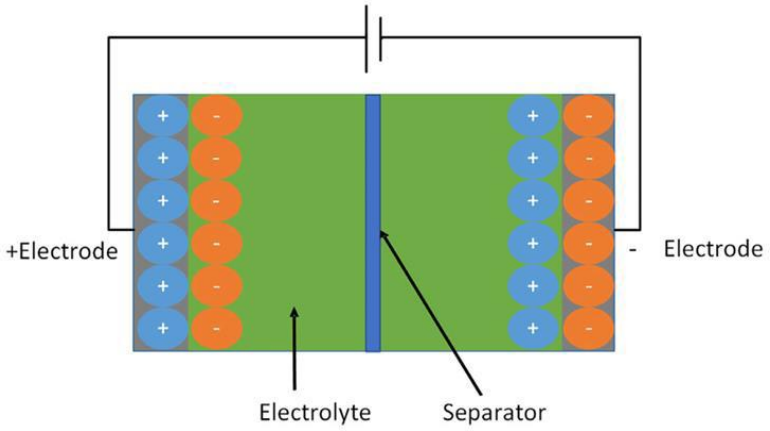

Figure 2.2 Schematic representation of EDLC [21]

2.5.2 Pseudocapacitors

Pseudocapacitors, distinguished as faradaic supercapacitors, deviate from electric double-layer capacitors (EDLCs) in their operational mechanism [22]. Unlike EDLCs, pseudocapacitance in these supercapacitors originates from rapid and reversible faradaic (electrochemical) processes occurring at or near the electrode surface, as depicted in **Figure 2.3** [23]. In pseudocapacitors, the flow of charge through the double layer involves faradaic currents traversing the supercapacitor unit, unlike the non-faradaic process in EDLCs [24].

This faradaic mechanism elevates the energy density and specific capacitance in pseudocapacitors compared to EDLCs. However, pseudocapacitors typically exhibit lower power density and less robust cycle stability than their EDLC counterparts. Commonly used pseudocapacitive materials include metal oxides such as RuO_2 and MnO_2, which are prevalent due to their effective faradaic reactions [25] [26]. These materials contribute significantly to the enhanced capacitance and energy storage capabilities of pseudocapacitors.

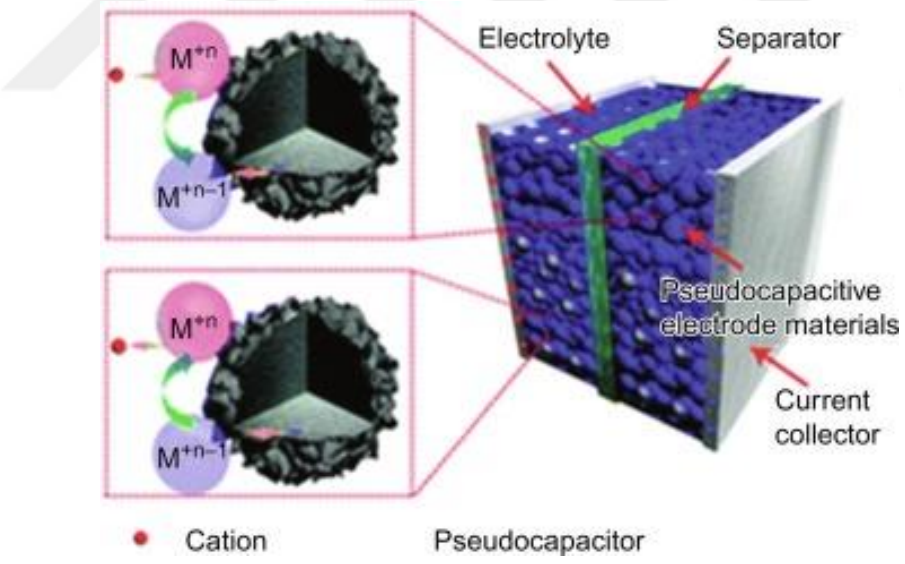

Figure 2.3 Sketch definition of pseudocapacitors [26]

2.5.3 Hybrid Supercapacitors

Hybrid supercapacitors stand out for their ability to store more energy while keeping the power output high [27]. These supercapacitors are better than both the regular double-layer capacitors and the faradaic supercapacitors in how much charge they can hold. Their special feature is the combination of two types of capacitors in one – one

that stores energy through electric fields (like in a regular capacitor) and another that stores energy through chemical reactions [28].

This mixed approach makes hybrid supercapacitors very promising for the future. They are especially useful in applications like electric cars and devices that need a lot of power [29]. **Figure 2.4** shows a diagram of a hybrid supercapacitor, highlighting how it works and its advantages.

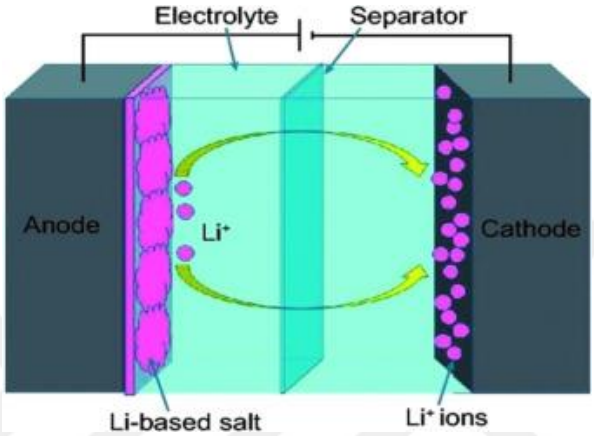

Figure 2.4 Schematic illustrator of hybrid supercapacitor [29]

2.6 Electrodeposition

In electroplating, metal ions are directed towards charged electrodes in an electric field, with minimal chemical additives involved. This process, known as electrodeposition, is highly efficient for purifying water with low levels of contaminants, as it relies on electrically driven ion movement rather than random diffusion [30]. This method can effectively extract specific pollutants from large volumes of complex wastewater. Furthermore, electrodeposition generates high-energy electrons that act as reducing agents, converting metal ions into solid form. The key benefits of electrodeposition in purifying water include its high efficiency, minimal secondary pollution, and simplicity of operation.

Electrodeposition typically uses a setup with three distinct electrodes: a working electrode, a counter electrode, and a reference electrode [31]. The working electrode is the focal point where metal ions accumulate, forming a layer through electrochemical reactions influenced by the current or voltage applied.

2.7 Supercapacitor Electrolytes

In the configuration of a three-electrode system, the roles of the counter, working, and reference electrodes are integral to the process. In the context of supercapacitors, the electrolyte emerges as a crucial component, playing a pivotal role in facilitating charge transport and maintaining the balance between anion and cation electrodes [32]. The interplay between electrodes and electrolytes significantly influences the state of the electrode-electrolyte interface and the structural integrity of the active materials in all electrochemical reactions. Therefore, the properties of the electrolyte-solution system are fundamental in determining the electrochemical performance of a supercapacitor. A well-chosen electrolyte can significantly enhance a supercapacitor's power density, energy density, and cycle longevity. **Figure 2.5** illustrates the types of electrolytes commonly used in supercapacitors and their role in the electrodeposition process [33] [34].

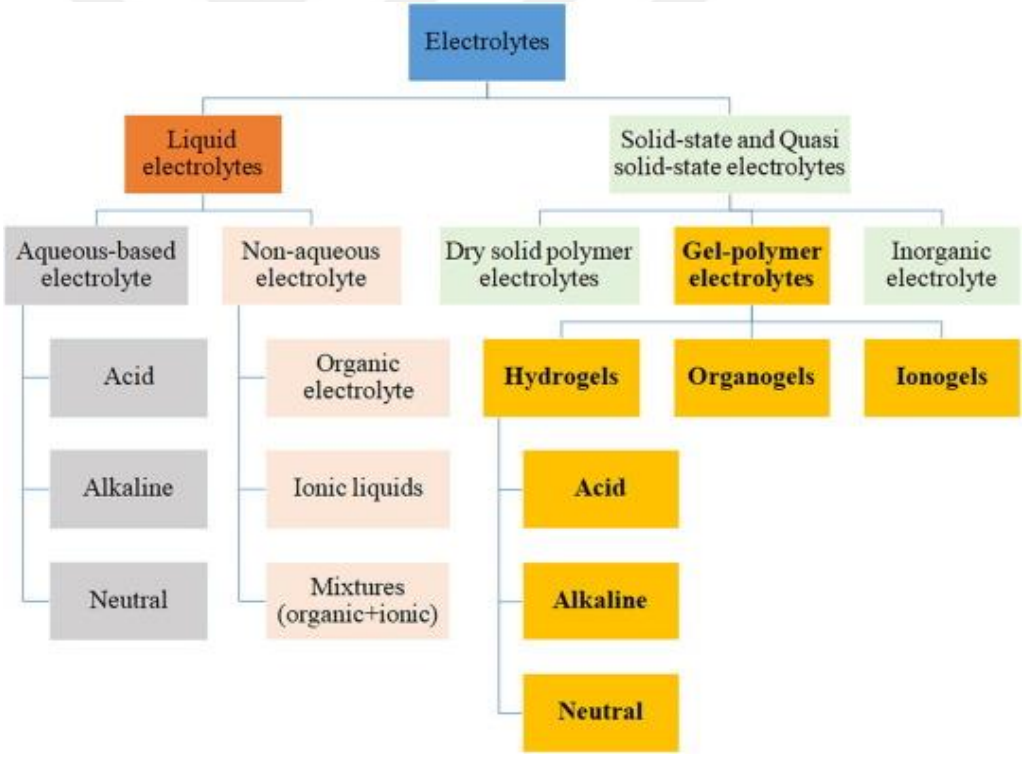

Figure 2.5 Diagram of electrolytes typically utilized in supercapacitors [33]

2.7.1 Conventional Electrolytes

In supercapacitors, conventional electrolytes play a crucial role in determining performance and energy density. Aqueous electrolytes, known for their high ionic conductivity, are limited by a narrow voltage window of about 1 V, constraining the energy density of supercapacitors [35]. Conversely, non-aqueous electrolytes can

operate at higher voltages (up to 4 V), offering increased energy density but at the cost of reduced conductivity and cycle stability [36]. Solid-state electrolytes, while eliminating the risk of leakage, often suffer from lower ionic conductivity, impacting the efficiency of supercapacitors [37]. The selection of an electrolyte is therefore a critical decision in supercapacitor design, balancing factors like operational voltage, conductivity, and stability to meet specific application needs. This balance is key to advancing supercapacitor technology and enhancing their performance in energy storage systems.

2.7.2 Ionic Liquids

Paul Walden first identified ionic liquids in 1914, marking a significant milestone in the field of chemical research [38]. Ionic liquids are essentially salts in a liquid state or those with a melting point below 100°C. This characteristic distinguishes them from traditional molten salts, which typically require higher temperatures to dissolve. Due to their expansive potential window and superior conductivity, molten salts have been a popular choice for extracting various metals like lithium, sodium, and titanium [39]. However, the high melting point and stringent application conditions have limited their utility, shifting the focus to ionic liquids in recent research. Unlike conventional liquids such as water or gasoline, which are primarily composed of neutral atoms, ionic liquids consist mostly of ions and transient ion pairs. These liquids are known for their non-flammability, high conductivity, extensive potential range, and broad thermal stability [40]. Over the past two decades, the unique properties of ionic liquids have increasingly captured the interest of the scientific community, leading to a surge in research and potential applications [41] .

2.7.3 Deep Eutectic Solvents

Deep Eutectic Solvents (DES) have emerged as a promising alternative to conventional electrolytes in supercapacitors, offering unique advantages in terms of environmental friendliness, cost-effectiveness, and electrochemical performance. DES are typically composed of two or more components, such as a quaternary ammonium salt and a hydrogen bond donor, which form a eutectic mixture with a melting point much lower than that of the individual components. This unique property allows DES to operate at ambient temperatures while providing high ionic conductivity and wide electrochemical windows. The use of DES in supercapacitors has been explored for

enhancing the device's energy density and cycle stability. The incorporation of DES in supercapacitors represents a significant step towards developing more sustainable and efficient energy storage devices, aligning with the global push towards greener technologies [42].

2.8 Characterization of Supercapacitor Materials

2.8.1 X-Ray Diffraction (XRD)

X-ray diffraction (XRD) is a powerful, non-destructive analytical technique used for identifying the crystallographic structure and phase composition of materials. This method allows for the analysis of properties like particle size, preferential orientation, and the crystalline structure of powder samples [43]. X-rays used in this technique have wavelengths ranging from 0.1 Å to 100 Å, facilitating detailed exploration of the sample's structure.

The process involves generating a pattern by analyzing the sample, which can then be compared against a known database to identify the phases present within the sample. Additionally, XRD can be utilized to determine the relative quantitative ratios of the components in the sample. Advanced methods such as Rietveld analysis are often employed for this purpose, offering a comprehensive understanding of the sample's composition and structure [44].

2.8.2 Fourier Transform Infrared Spectroscopy (FTIR)

Fourier Transform Infrared Spectroscopy (FTIR) has become an indispensable tool in material science, offering detailed insights into the molecular structure and composition of materials. FTIR works by detecting the wavelengths at which a material absorbs infrared light, corresponding to the vibrations of the molecules within the material. This technique is particularly valuable for identifying organic compounds, polymers, and inorganic materials, as well as for studying surface modifications and interactions. Recent advancements in FTIR technology have expanded its applications in various fields, including biomedical applications for analyzing human blood, biochemical studies of organic materials, geological research in clay mineralogy, and ensuring product safety and traceability in wood pellet production. FTIR's versatility and precision make it a powerful tool in material science, aiding in the characterization and analysis of a wide range of materials.[45].

2.8.3 Scanning Electron Microscopy (SEM)

The Scanning Electron Microscope (SEM) is an essential tool in material science, providing high-resolution images of sample surfaces by using a focused beam of electrons. When electrons interact with atoms in the sample, they generate various signals that reveal detailed information about the sample's topography and composition. SEM operates through raster scanning, where the electron beam's position correlates with the detected signal to create an image. Capable of achieving resolutions greater than 1 nm, SEM is adept at examining both dry and electrically conductive samples in high vacuum, as well as non-conductive samples in low vacuum settings. Images in SEM are predominantly produced by secondary electrons emitted from sample atoms energized by the electron beam. The emission of these secondary electrons largely depends on the beam's angle of incidence and the surface topography of the sample, making SEM a powerful tool for analyzing material surfaces at the nanoscale.[46], [47].

2.9 Electrochemical Analysis of Supercapacitors

2.9.1 Chronoamperometry

Chronoamperometry is a key electrochemical technique used for exploring the dynamics of chemical changes, diffusion mechanisms, and adsorption processes. In this method, a specific potential step is applied to an electrode, and the corresponding current is measured over time. This technique is particularly useful for studying both single and double potential step processes [48]. The chronoamperometry experiment can also be employed to detect or monitor various events. In cases where the response does not adhere to the Cottrell equation, the process is simply referred to as "amperometry." Typically, before starting the experiment, the electrode is held at a potential where no faradaic (redox) process occurs. The potential is then shifted to a level where a redox reaction takes place, marking the beginning of the chronoamperometry experiment. This moment of potential shift is designated as zero time. Chronoamperometry is a valuable tool for accurately determining one or more parameters in the Cottrell equation (such as electrode size, diffusion coefficient, or concentration of the sample), especially when the contributions from adsorbed material are negligible and the other variables are known. This makes chronoamperometry a versatile and powerful technique for investigating electrochemical reactions and the properties of materials in an electrochemical context.

2.9.2 Chronocoulometry

Chronocoulometry, an advanced electrochemical technique, plays a pivotal role in the detailed analysis of redox reactions and material properties. This method involves the application of a constant potential to an electrochemical cell and the precise measurement of the charge passed over time. By doing so, it yields critical insights into the diffusion coefficients, surface coverage, and reaction mechanisms at the electrode-electrolyte interface. Chronocoulometry is particularly effective in studying the kinetics of thin films, corrosion processes, and modifications on electrode surfaces. The technique's ability to provide quantitative data on the amount of material deposited or dissolved at the electrode surface makes it invaluable in material science research. It has been used to explore novel approaches in electroanalysis, particularly in the extraction and analysis of solid precipitates [49], to measure the diffusion constants of thin coating layers [50], and in research on solid oxide fuel cells, specifically studying the effect of sulfur on porous Ni-YSZ anodes. Chronocoulometry's ability to provide detailed electrochemical data makes it a powerful tool in advancing research across various fields, including material science, energy storage, and electrochemical engineering.[51].

2.9.3 Cyclic Voltammetry

Cyclic Voltammetry (CV) is the most widely used technique in electrochemical analysis, offering valuable insights into the redox properties of the analyte and the behavior of the electrode itself. By examining the shape and peak positions on cyclic voltammogram curves, one can deduce the reversibility of the electrochemical reactions taking place—whether they adhere to Nernstian behavior or are irreversible in nature [52]. cyclic voltammogram also enables the study of additional reaction dynamics, including mass transport phenomena. It is typically the preliminary assessment performed on electrochemical sensors to evaluate their capacity for selective detection. However, due to its higher detection and quantification thresholds compared to other voltammetric methods, cyclic voltammogram may not be the most effective for quantitative analysis. In a conventional setup for these measurements, an electrolyte solution encompasses a triad of electrodes: the counter electrode, the reference electrode, and the working electrode, which are integral to the analytical process [53].

CHAPTER 3

EXPERIMENTAL PROCEDURES

3.1 Used Devices, Tools, and Materials

Preparation Materials

1. **Graphite Substrate**: A substrate with 99% purity, to be meticulously cleaned for use in the experiment.
2. **Sandpaper (600 Microns)**: Employed to smooth the graphite surface.
3. **Transparent Tape**: Applied to cover and prepare the graphite substrate surface.
4. **Scissors**: Utilized for cutting the transparent tape to appropriate sizes for covering the graphite substrate.
5. **Ruler**: A measuring tool for checking the conductivity of the tape-coated graphite surface.

Electrochemical Measurement Materials

1. **Reference Electrode:** In aqueous solutions, an electrode with an AgCl layer on Ag wire and saturated potassium chloride electrolyte in a glass body is used. For DESs, a Platinum wire serves as a direct reference electrode as shown in **Figure 3.1**.
2. **Counter Electrode:** Titanium-coated platinum (Pt) mesh.
3. **Working Electrode:** tapes are used as graphite substrates in electrochemical experiments for this study.

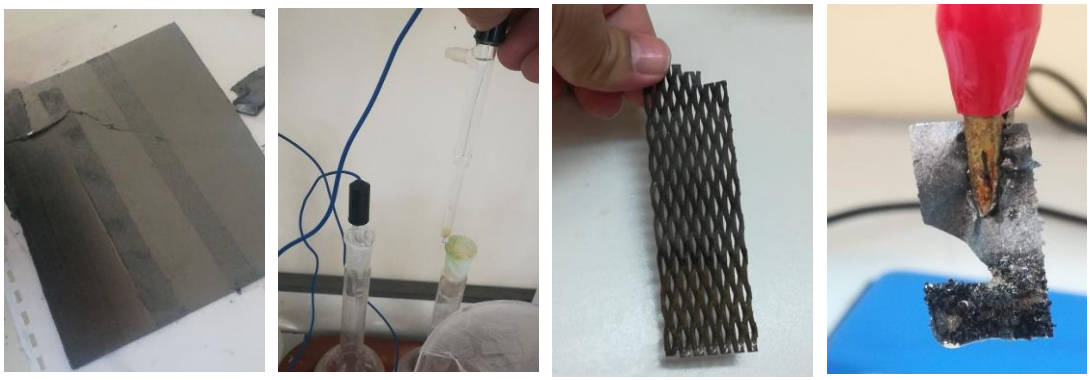

a) Graphite Substrate **b) Reference Electrode** **c) Counter Electrode** **d) Working Electrode-coated**

Figure 3.1 Photos of materials used in the experiments.

Table 3.1 Catalogue of Laboratory Apparatus and Reagents Employed in the Experimental Investigations

Instrumentation/Reagent	Application Description
Analytical Balance (±0.0001 g)	Utilized for the determination of material mass with high precision, critical for quantitative analytical procedures.
Temperature-Controlled Heating/Stirring Unit (±3 °C)	Applied to maintain precise thermal conditions for reaction mixtures, facilitating controlled reaction rates and uniformity.
Laboratory Thermometers	Essential for precise thermal monitoring of reaction systems, enabling the investigation of temperature-dependent reaction kinetics.
Disposable Weighing Dishes	Implemented for the containment and accurate massing of reagents, mitigating the risk of sample adulteration.
Laboratory Spatulas	Employed for the transference of solid reagents, minimizing contamination, and ensuring volumetric precision.
Glass Beakers	Standard glassware for compound synthesis and solution preparation, indispensable for stoichiometric accuracy and process visualization.
Stirring Rods	Glass implements used for promoting homogeneity in reaction mixtures, essential for consistent experimental conditions.
Magnetic Stir Bars	Integral to stirring operations within a controlled temperature setting, ensuring isotropic mixing and thermal distribution.
Dryer	Utilized for the dessication of materials post-washing, imperative for the precision in subsequent analytical measurements.
Protective Laboratory Gloves	Employed to handle sensitive materials and equipment, ensuring protection from chemical exposure and maintaining experimental sterility.
Safety Goggles	Essential personal protective equipment to prevent eye exposure to hazardous materials and reactions.
Distilled Water	Reserved for final-stage cleaning of glassware to eliminate residual impurities, safeguarding the integrity of chemical analyses.

3.1.1 Chemicals in the Experiment

This table enumerates the reagents utilized in the experimental studies conducted for this thesis, detailing their respective purities and sources.

Table 3.2 Chemicals Employed in Experimental Procedures

No	Chemical Name	Purity	Supplied by
1	Manganese (II) Chloride Dihydrate ($MnCl_2 \cdot 2H_2O$)	≥98%	Merck
2	Choline Chloride ($HOCH_2CH_2N(CH_3)_3Cl$)	≥98%	Alfa Aesar
3	Monoethylene Glycol ($C_2H_6O_2$)	High Purity	Neobiğlu
4	Potassium Hydroxide (KOH)	≥90%	Tekkim
5	Sodium Sulfate (Na_2SO_4)	≥90%	Merck

The reagents listed were selected for their high purity levels to ensure the reliability of experimental results and consistency of the study. Each reagent was sourced from reputable suppliers known for their quality assurance in chemical products.

3.2 Preparation of Electrodes

In the preparation phase of the graphite-coated flexible tape as shown in **Figure 3.2** electrode, essential for initiating the principal experimental process, the following methodical stages are conducted:

- **Surface Cleaning:** Initially, the graphite substrate, designated for sample extraction, undergoes a cleaning process. A clean napkin is employed to meticulously wipe the surface, ensuring the removal of all visible contaminants, and preparing it for subsequent treatment.

- **Sanding Process**: After cleaning, the graphite surface is subjected to a sanding procedure using 600-micron sandpaper. This process is continued until the graphite attains a uniformly flat structure, resulting in a substrate surface that is both smooth and homogeneous.

- **Taping Process:** Following the sanding, the now clean and flattened graphite surface is covered with transparent tape. This crucial step prepares the substrate for further processing stages.
- **Pre-film Formation:** The tape is then gently pressed onto the graphite surface to ensure initial adherence and uniform contact across the surface.

- **Film Formation:** At this juncture, the tape is firmly bonded to the graphite surface. This critical step ensures a strong bond and the elimination of air bubbles between the tape and the surface.

- **Full Film Formation:** The tape is meticulously adhered to the graphite surface, with special attention to avoiding any loose edges or gaps, thus achieving a tight and seamless bond.

- **Flexible Graphic Film Production:** Resulting from the taping process, the graphite surface becomes enveloped with tape, leading to the formation of a flexible graphic film. This film is subsequently detached from the graphite surface to produce a thin, flexible substrate.

- **Sample Collection:** The flexible graphic tape film is measured and cut into the required size, typically 1 cm^2. These samples are crucial for the forthcoming experimental steps, enabling the preliminary testing procedures for electrode coating.

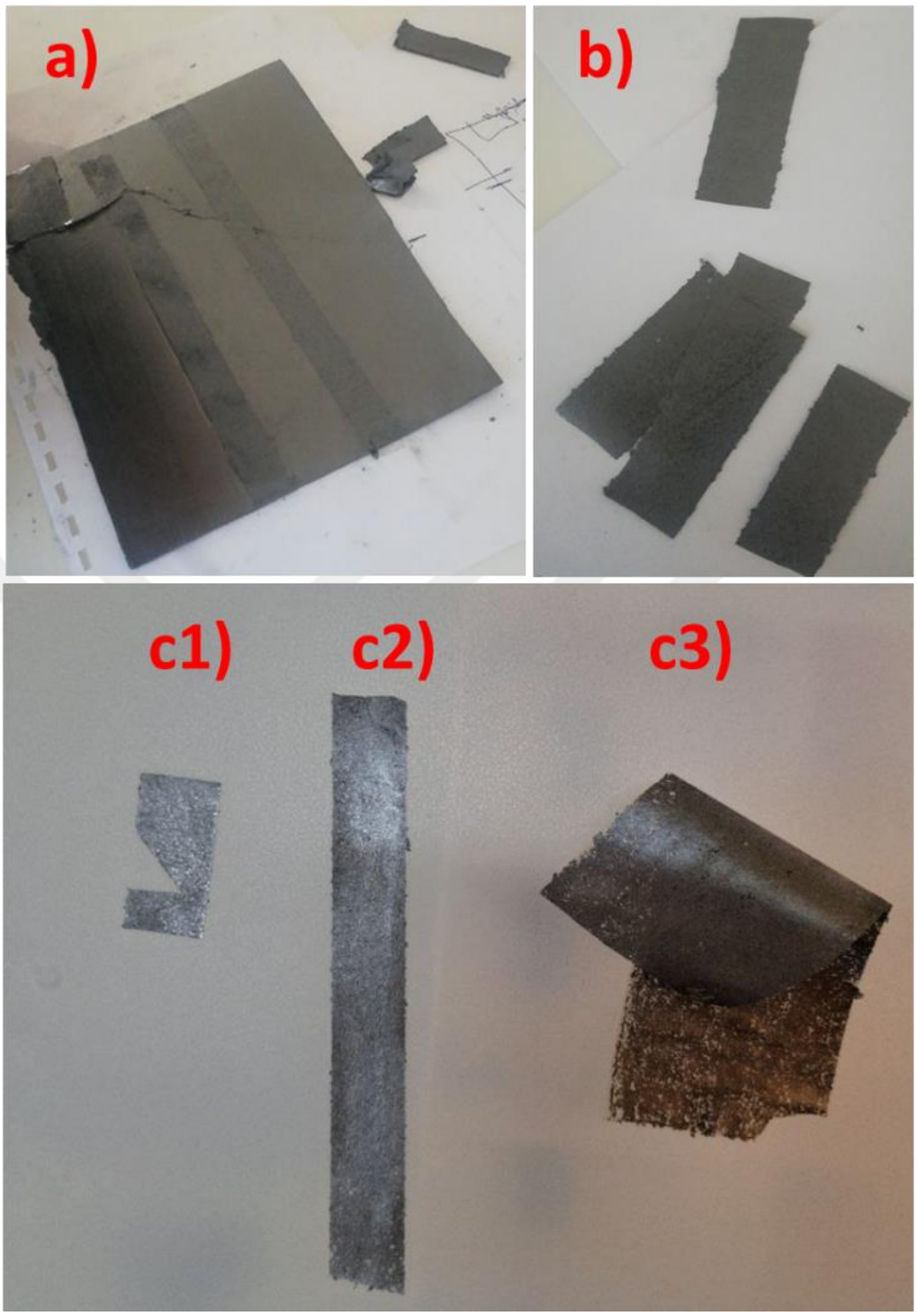

Figure 3.2 Photos of working electrodes' preparation phases

3.3 Preparation of Deep Eutectic Solvent

At the outset, the preparation method for Ethaline, a type of Deep Eutectic Solvent, was selected. The primary ingredients for creating Ethaline are Choline Chloride (ChCl) and Ethylene Glycol (EG) According to the following steps:

- **Weighing Chemical Components and Preparing the Solution**: To begin, Choline Chloride (ChCl) and Ethylene Glycol (EG) were separately weighed using precision scales. The total amounts measured were 100 grams of Choline Chloride (ChCl) and 88 grams of Ethylene Glycol (EG). Following this, 88 grams of Ethylene Glycol (EG) were poured into a beaker, to which 100 grams of Choline Chloride (ChCl) were then added, completing the measurement process.
- **Preheating Phase:** Initially, the Choline Chloride (ChCl) and Ethylene Glycol (EG) blend was heated to 75°C for a duration of 15 minutes to formulate the Ethaline solution. This preheating stage was deemed complete when the mixture attained a temperature close to 70°C.
- **Mixing and Heating Process**: The mixture of Choline Chloride (ChCl) and Ethylene Glycol (EG) was stirred and heated over an extended period at a set temperature of 60°C until it formed a homogeneous structure. After about 180 minutes, the formation of a consistent Ethaline mixture at 60°C was verified using a thermometer. This marked the final step in the preparation of the ionic liquid, concluded by cooling the mixture to room temperature.

In conclusion, the Ethaline solution was initially heated to 75°C in the preheating step. It was then mixed and heated at 60°C until it achieved a homogeneous consistency. The homogeneous Ethaline solution, obtained after roughly 180 minutes, was then allowed to cool down to room temperature, completing the ionic liquid preparation.

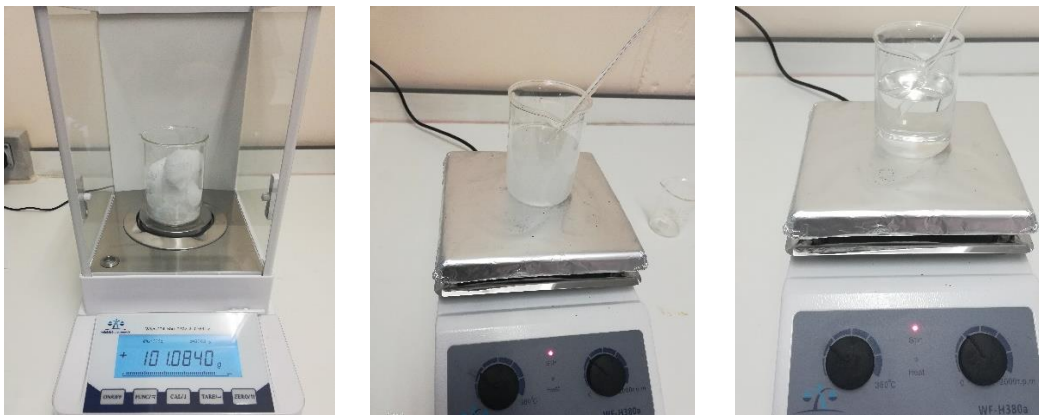

a) Weighing Choline Chloride b) Heating and Stirring the Mixture c) Finishing Preparation

Figure 3.3 Photos of Ethaline preparing steps

3.4 Element Selection and Preparation for Electrode Modification

In the process of modifying electrodes, the use of the manganese (Mn) element was chosen to enhance the graphite substrate. Manganese was identified as beneficial in improving both the characteristics and efficacy of the chosen coating technique.

- **Weighing of Chemical Components and Solution Preparation**: $MnCl_2$ powder was accurately weighed using precision balances. A total of 0.7 grams of $MnCl_2$ was measured and added to 50 mL of Ethaline to prepare solutions with a concentration of 0.1 M $MnCl_2$.
- **Preheat Stage:** The mixture of $MnCl_2$ and Ethaline was preheated to 75°C for 15 minutes in a beaker. The preheating phase was deemed complete when the temperature of the mixture reached approximately 65°C.
- **Mixing and Heating Stage:** Once the heater was set to 60°C, the solution was stirred, and heating was continued to achieve a uniform structure over an extended period. After about 150 minutes, the temperature of the mixture was checked with a thermometer. The desired homogeneous structure was confirmed when the temperature stabilized around 60±2 °C, marking the conclusion of the process. As a result, Ethaline solutions with a $MnCl_2$ concentration of 0.1 M were successfully produced.

a) Mixture Components b) Adding $MnCl_2$ to Ethaline c)Mixing and Heating

Figure 3.4 Photos illustrate preparing 1M $MnCl_2$ in Ethaline

3.5 Preparation of Electrolytes

- **1 M Na_2SO_4 Electrolyte Solution Preparation:** To prepare the 1 M Na_2SO_4 electrolyte solution, 71.02 grams of Na_2SO_4 (Sodium sulphate) were accurately weighed. This was followed by the addition of the chemical to 500 mL of distilled water, ensuring a total solution volume of 500 mL. During this addition, continuous stirring was employed to promote the formation of a homogeneous mixture. The process was continued until the Sodium sulphate (Na_2SO_4) completely dissolved in the water, resulting in a successfully prepared 1 M Na_2SO_4 solution.
- **1 M KOH Electrolyte Solution Preparation:** For the 1 M KOH solution, 28.05 grams of KOH (Potassium hydroxide) were measured. The KOH was gradually added to 500 mL of distilled water. Careful and slow addition of the chemical was crucial to ensure complete mixing and dissolution. Continuous stirring was maintained throughout the process to achieve a homogeneous mixture. Once the Potassium hydroxide (KOH) fully dissolved in the water, the 1 M KOH solution was successfully obtained.

3.6 Study of Manganese-Coated Graphite Samples for Supercapacitor Electrodes with Electrochemical Characterization Techniques

In this research, flexible supercapacitor electrodes were fabricated by electrochemically depositing manganese onto graphite substrates. This deposition was achieved through a potentiostatic method, applying various potentials to coat the graphite electrodes with manganese. The study involved a detailed examination of both the coated and uncoated electrodes, focusing on their chemical, structural, and morphological characteristics. Following the modification, the electrodes were immersed in electrolyte solutions of potassium hydroxide (KOH) and sodium sulphate (Na_2SO_4). This step was crucial to assess their electrochemical behaviour. A range of electrochemical characterization techniques, including chronocoulometry, chronoamperometry, cyclic voltammetry, and cyclic polarization, were employed to investigate the electrochemical properties of both the uncoated pure graphite and the manganese-coated graphite electrodes. These investigations were particularly focused on determining the capacitance values of the electrodes, which are key indicators of their performance in supercapacitor applications.

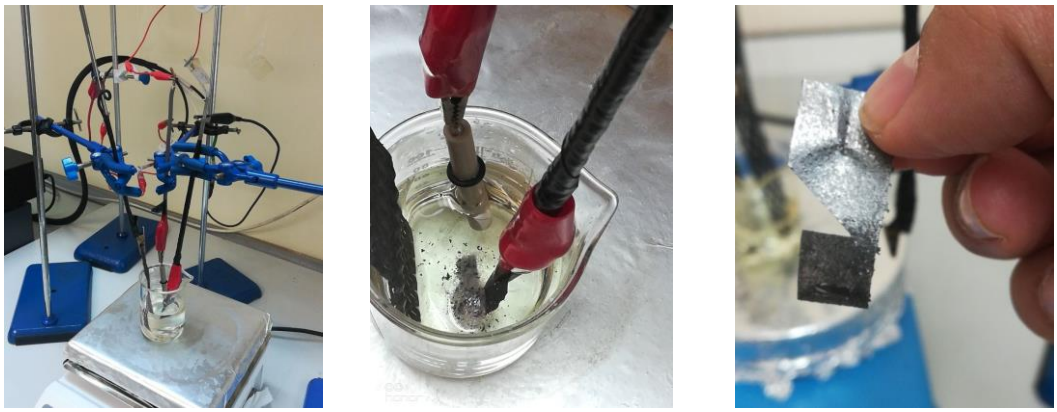

a) Experiment Installation b) Running Coating Process c)Working Electrode After Coating

Figure 3.5 Photos illustrate graphite tape coating

3.6.1 Chronocoulometry Analysis

Chronocoulometry analysis was employed to study the electrochemical deposition of manganese on graphite tape electrodes. Potentials of -1.5 V, -2 V, and -2.5 V were applied to the electrodes immersed in a 0.1 M $MnCl_2$ solution prepared in Ethaline. The solution was maintained at 60 °C for 500 seconds. This method allowed for the observation of manganese growth on the graphite electrodes. The analysis was conducted using a VersaSTAT 3 potentiostat from Princeton Applied Research, manufactured by AMATEK Company (USA). This study provided insights into the growth characteristics of manganese on graphite electrodes, including the alloy's capacity and charging duration, essential for optimizing the electrochemical plating process.

3.6.2 Chronoamperometry

For the electrode coating process, a 0.1 M $MnCl_2$ solution in Ethaline was used, heated to 60°C. The graphite tape served as the working electrode, with platinum wire as the reference electrode and a platinum part as the counter electrode. Electrodeposition was carried out for 500 seconds at potentials of -1.5 V, -2 V, and -2.5 V using the potentiostatic method. The process was controlled using the VersaSTAT 3 potentiostat. Chronoamperometry provided valuable data on various optimization parameters, including the kinetics and rate of electrochemical reactions and the electrode surface capacity.

3.6.3 Cyclic Voltammetry

Cyclic voltammetry tests were conducted to evaluate the electrochemical performance of Mn-coated graphite tape electrodes. These tests were carried out using the VersaSTAT 3 potentiostat from Princeton Applied Research, manufactured by AMATEK Company (USA), in a three-electrode system. An Ag/AgCl reference electrode and a titanium working electrode with a platinum coating were used in a saturated KCl solution. The electrolytes employed for these tests were 1M KOH and 1M Na_2SO_4, used separately.

The electrodes were coated in a 0.1 M $MnCl_2$ solution in Ethaline at 60°C for 500 seconds. The cyclic voltammetry analysis involved two sets of scanning cycles:

The first set consisted of 20 scanning cycles performed on the Mn-coated graphite electrodes between -0.8 V to 0.2 V at a constant scan rate of 50 mV s^{-1}. The second set included 20 scanning cycles at various scan rates, detailed as follows:

a) 3 cycles at 100 mV s^{-1},
b) 3 cycles at 50 mV s^{-1},
c) 3 cycles at 25 mV s^{-1},
d) 2 cycles at 10 mV s^{-1},
e) 9 cycles at 100 mV s^{-1}.

The cyclic voltammetry plots from both sets of scans were crucial in determining the oxidation and reduction peak values. Graphs were created using the logarithm of these peak values and the logarithm of the applied potential scanning rates. This comprehensive approach provided a thorough exploration of the results, offering valuable insights into the electrochemical behavior of the Mn-coated graphite tape electrodes under both constant and varying scan rates.

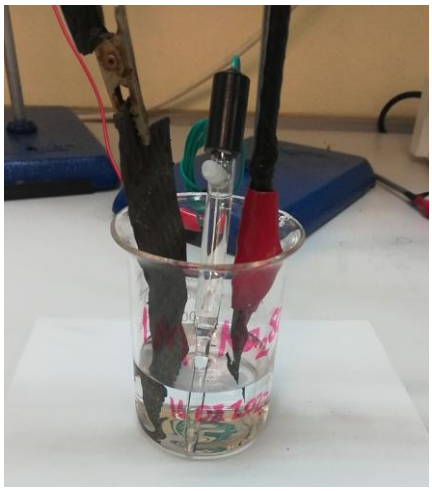

a) Experiment Installation

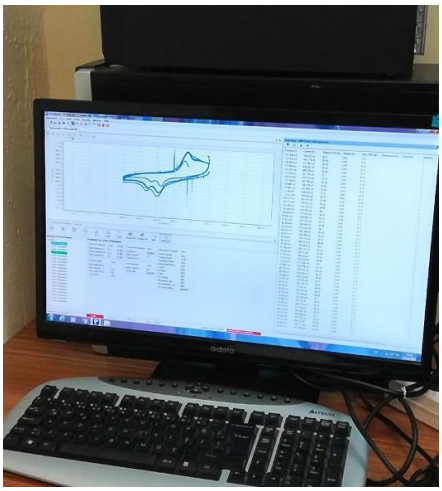

b) Monitoring The Process Through PC

Figure 3.6 Photos of conducting Cyclic voltammetry Test

3.7 Study of Manganese Coated on Graphite Sample Non-Electrochemical Characterization Techniques

This experimental study has been primarily focused on the performance of flexible electrodes, a pivotal aspect in the development of advanced energy storage technologies. The investigation centered on graphite samples coated with manganese, which are key materials in the fabrication of this electrode. To this end, a suite of characterization techniques was employed, encompassing X-ray diffraction (XRD), Fourier transform infrared spectroscopy (FTIR), and scanning electron microscopy (SEM). XRD was instrumental in assessing the crystalline structure of the electrodes, while FTIR provided valuable information regarding their compositional makeup. Additionally, SEM was utilized to examine surface morphology in detail.

These characterization methods enabled a comprehensive analysis of the composition, structural attributes, and surface features of the fabricated flexible electrodes. The results gleaned from these characterizations have been instrumental in shedding light on the design and optimization of the electrodes' performance. This exploration represents a fundamental step forward, laying the groundwork for future research endeavors aimed at enhancing the development of flexible electrode technologies.

3.7.1 X-Ray Diffractometer (XRD) Analysis

Prior to discussing the experimental details, it is essential to comprehend the basic characteristics of X-rays, a significant segment of the electromagnetic spectrum. X-rays are distinguished by their higher intensity, increased frequency, and shorter wavelengths compared to ultraviolet radiation. These properties, which align closely with the principles of crystallography, highlight the suitability of X-rays for investigating the crystalline structure of materials.

In this experiment, the Automate II XRD instrument, manufactured by Rigaku Company in Japan, was utilized. This device operates by directing X-rays towards the samples and measuring the intensity of the reflected rays. The analysis of these intensity peaks is crucial for identifying variations in the crystal structure of the samples. The samples were exposed to X-rays with a wavelength of 1.54 Å from a CuKα source, and the analysis was conducted over an angular range of 2° to 80°.

The focus of the study was on analyzing the manganese modification coatings applied to the graphite surfaces of the samples at various voltage values. The primary objective was to determine the changes in the crystal structure of the electrodes. This analysis has provided essential insights into the characteristics, performance, and crystalline formations of the electrodes, enhancing our understanding of their properties.

3.7.2 Scanning Electron Microscopy (SEM)

In this research, Scanning Electron Microscopy (SEM) was employed to meticulously examine both manganese-coated and bare graphite electrodes. The SEM technique provided high-resolution images that highlighted the homogeneity and structural details of the manganese coating in comparison to the uncoated graphite surfaces. These observations were pivotal in discerning the influence of the manganese coating on the electrodes' electrochemical properties, as well as in evaluating the intrinsic qualities of the bare graphite. This analysis significantly enriched our understanding of their roles and efficiencies in energy storage systems.

3.7.3 Fourier Transform Infrared Spectroscopy (FTIR) Analysis

Fourier Transform Infrared Spectroscopy (FTIR), which operates within the infrared region of the electromagnetic spectrum, was utilized in this study to characterize manganese-coated graphite tape electrodes. The Vertex 70v model FTIR, produced by the United States-based Bruker Company, was employed for this purpose. FTIR is adept at analyzing a diverse range of materials, including solids, liquids, and gases, through the absorption and emission of infrared light. In the experimental setup, the graphite tape electrodes were coated with a 1M $MnCl_2$ solution in Ethaline at 60°C for 500 seconds. The coating was applied at voltage values of -1.5 V, -2 V, and -2.5 V. Post-coating, both the manganese-coated and bare graphite tape samples underwent FTIR analysis. Infrared rays were directed at the samples, and the transmission of these rays through the surfaces was meticulously recorded. The resulting data were then graphically represented and analyzed. This FTIR analysis was particularly crucial in investigating the presence and structural composition of the manganese coating on the electrode surfaces. The findings from the FTIR spectroscopy analysis played a significant role in assessing the stability and quality of the coating process, thereby contributing to our understanding of the electrodes' suitability for energy storage applications.

CHAPTER 4
RESULTS AND DISCUSSION

4.1 Manganese Growth on Flexible Graphite

Uncoated graphite was immersed in Ethaline electrolyte having Mn^{2+} and pure Ethaline for cyclic voltammetry analyses (**Figure 4.1**). The black line in **Figure 4.1** shows the cyclic voltammogram responses of graphite containing Mn^{2+} ions in Ethaline. The results represented by the black line indicate significant redox reactions in the presence of Mn^{2+}. Oxidation of manganese was started at around -0.1 V, and a reduction peak is observed around -0.5 V. This finding suggests that the deposition of Mn onto the electrode surface could be possible.

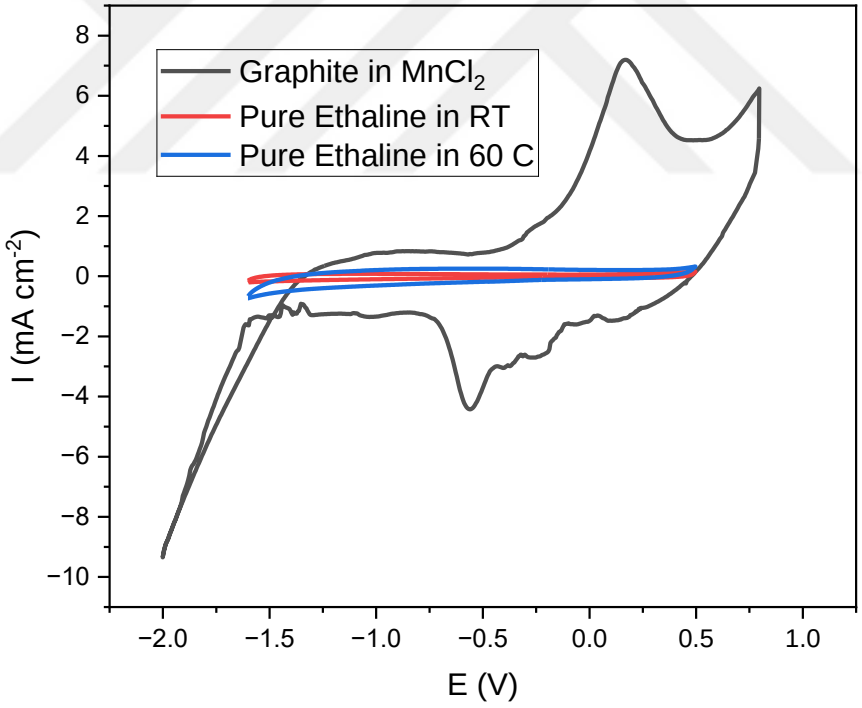

Figure 4.1 Cyclic voltammogram results of bare graphite in (black line) Ethaline having $MnCl_2$, (red line) pure Ethaline in Room Temperature and (blue line) pure Ethaline in 60 ^{o}C.

On the other hand, when examining the cyclic voltammogram results of pure Ethaline represented by the red and blue lines in the **Figure 4.1**, it is evident that experiments

conducted at 60°C could have higher current. Particularly, the results of graphite samples in Ethaline at 60°C are more pronounced compared to the redox findings at room temperature. This indicates that the higher temperature facilitates faster and more effective diffusion of ions onto the electrode surface. However, the current densities of electrode in pure Ethaline in both temperature is much lower than that of the electrode cycling in Ethaline with manganese ions.

In the realm of electrochemical deposition dynamics, advanced analytical experiments were conducted to explore the manganese electrodeposition process onto graphite coated tapes. Utilizing a deep eutectic solvent of Ethaline with 0.1 M $MnCl_2$, these experiments provide a comprehensive understanding of the deposition conditions (especially growth potential). The insights gained from this study are crucial for optimizing the electrodeposition potential. As reduction of manganese started at around -1.5 V, the first growth potential was selected -1.5 V. The other growth potentials (-2.0 V and -2.5 V were selected to analyse the effect of growth potential on electrochemical behaviour of the resulting electrodes.

The chronoamperometry method was employed to conduct process analyses of the electrodeposition of manganese onto graphite tapes. This electrochemical process was achieved using AMATEK Company's (USA) VersaSTAT 3 potentiostat (by Princeton Applied Research) during the growth and cycling stages of electrochemical processes. Counter and reference electrodes were platinum and silver/silver chloride respectively when the electrolyte was aqueous solution. However, the reference electrode was silver wire when the electrolyte was ionic liquid.

In the chronoamperometry analysis, the deposition behavior of manganese on graphite coated tapes in an Ethaline solution having 0.1 M $MnCl_2$ was meticulously examined at a constant temperature of 60°C. Particularly at an applied potential of -2.5 V, the current density displayed a notable increase, reflecting a more notable manganese deposition process compared to that of -1.5 V potential. This is evidenced by a peak current density reaching as shown in **Figure 4.2**(a) and **Figure 4.2**(b) approximately to -10 mA/cm² after 500 seconds, indicating a robust and accelerated deposition. In contrast, the deposition at -1.5 V, with a peak current density near -0.25 mA/cm², suggests a more gradual and controlled manganese accumulation.

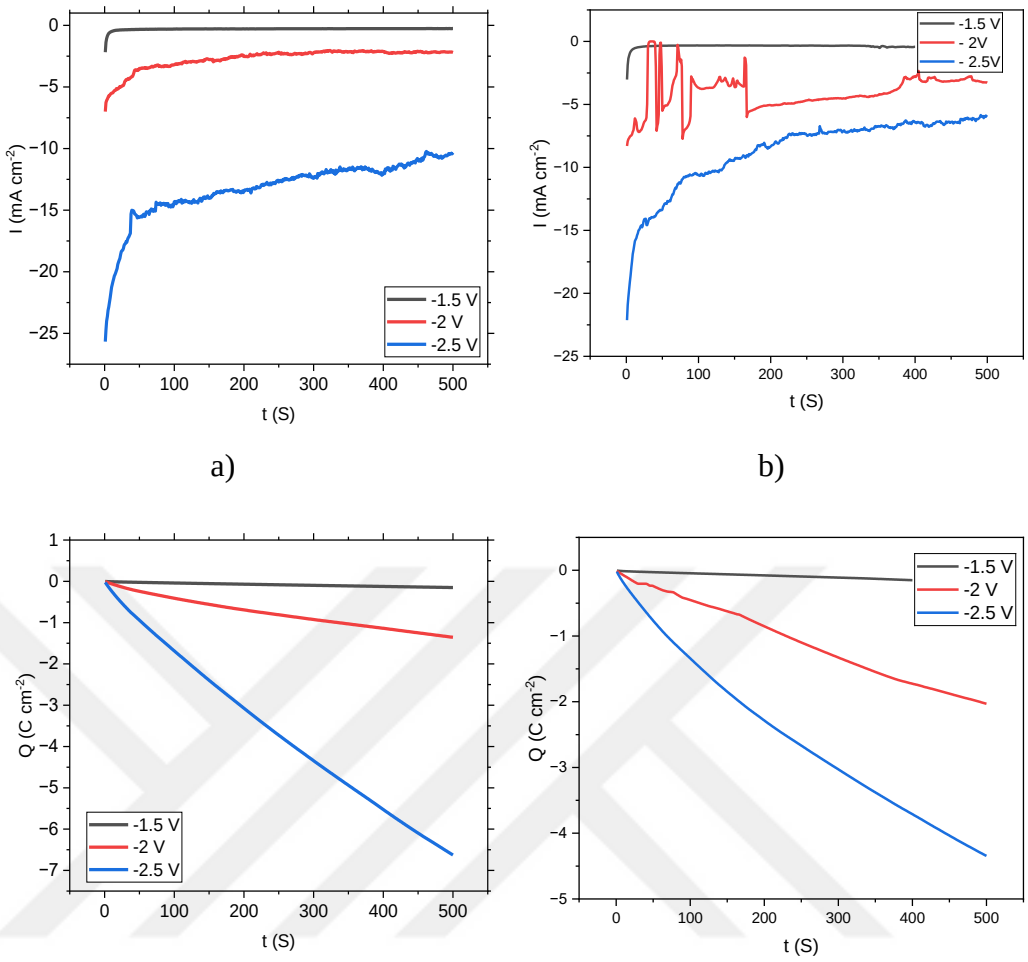

Figure 4.2 Chronoamperometry data for the electrode obtained by application of -1.5 V, -2 V and -2.5 V for transferring to a) Na_2SO_4 and; b) KOH. Chronocoulometry data for the electrode obtained by application of -1.5 V, -2 V and -2.5 V for transferring to c) Na_2SO_4 and; d) KOH. The growth of the Mn was conducted at 60° C for 500 seconds.

The chronocoulometry analysis provides a quantitative perspective on manganese deposition onto graphite-based tape samples. The observable trend in the data indicates that as the applied potential increases, there is a corresponding elongation in the time required for the deposition process to reach a state of stability. Specifically, at an applied potential of -2.5 volts, the system demonstrates a delayed stabilization compared to the -1.5 volts application, which stabilizes more rapidly.

This extended period required to achieve equilibrium at higher potentials is reflected in the charge accumulation pattern, which conveys an initial swift increase followed by a gradual leveling off. While higher potentials are associated with extended

stabilization times, the film was thicker meaning that the surface area could be higher. At higher potentials a more vigorous electrochemical activity could occur when the modified electrodes are cycled in KOH and Na_2SO_4. A denser manganese-based coating could be obtained on the graphite substrate. Bubbles were observed during electodepostion at higher negative potential as shown in **Figure 4.3**. This contributes to a less efficient deposition process because of hydrogen evolution reaction.

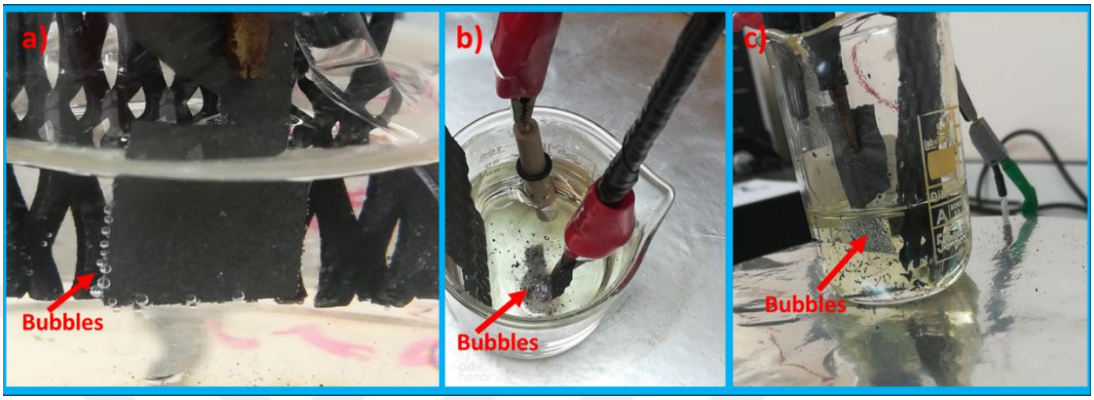

Figure 4.3 Photos of Bubbles Appeared During the Coating Process When Appling a)-2V; b)-2.5V and c) -2.5V

Hence, the chronocoulometry data not only substantiate the impact of applied potential on the kinetics of the electrodeposition process but also illustrate the trade-off between stabilization time and deposition efficiency as shown in **Figure 4.2**(c) and **Figure 4.2**(d). This nuanced insight aids in optimizing the electrodeposition protocol for superior coating performance on graphite electrodes.[54]. The coated graphite by Mn based film are illustrated in **Figure 4.4**.

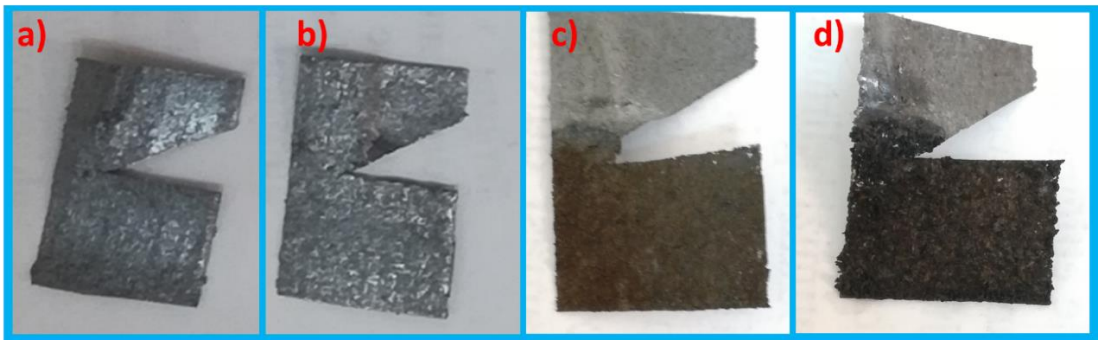

Figure 4.4 Photos of a) bare graphite and Mn coated graphite on tape from Ethaline Deep Eutectic Solvent by the application of b) -1.5 V; c) -2.0 V and; d) -2.5 V.

4.2 SEM Analysis of Flexible Electrodes

Graphite was attached to a tape, and it was used as a flexible substrate. Mn was coated on graphite layer from Ethaline ionic liquid by applying different potentials (-1.5 V, -2 V and -2.5 V) for 500 seconds at 60^{o}C. After obtaining Mn modified electrodes, they were transferred to KOH and Na_2SO_4. The electrochemical characteristics of the electrodes were tested after non-electrochemical characterisations (SEM, XRD and FTIR).

Bare graphite electrode (with magnification of 50 kX): The SEM image shown in **Figure 4.5** (a) and **Figure 4.5** (b) of the bare graphite electrode provides a foundational reference for understanding the effects of manganese electrodeposition. At 50,000x magnification, the bare graphite surface displays a smooth and homogeneous structure with minor natural imperfections. This pristine topography represents the initial state prior to any electrochemical modification, offering a critical baseline for comparison. The intrinsic qualities of graphite, such as its laminar structure characterized by flat, layered morphology, are apparent. As graphite is electrically conductive, it could be used as a substrate for electrochemical coatings. All graphites on tape were checked for conductivity by means of a multimeter.

Electrode obtained at -1.5 V (magnification: 50 kX): Under 50,000x magnification, the SEM images of the electrodes obtained at -1.5 V shown in **Figure 4.5** (c) and **Figure 4.5** (d) reveal the early stages of manganese deposition on the graphite electrodes. The sparse distribution of manganese formations suggests a nascent phase of electrodeposition, setting the foundation for subsequent layering and uniformity of the manganese coating. The minimal coverage at this stage is indicative of the initial interaction between the manganese and the graphite surface.

Electrode obtained at -2 V (magnification: 50.0 kX): the SEM images in **Figure 4.5** (e) and **Figure 4.5** (f) show a more uniform and continuous manganese layer. This stage represents a significant growth and progression in the electrodeposition process, where manganese structures begin to coalesce, forming a cohesive layer. The conductivity of the modified electrode was checked by a multimeter. The uniformity of Mn coating is essential for enhancing the electrode's electrochemical potential and its overall performance in energy storage applications.

Electrode obtained at -2.5 V (magnification: 50.0 kX): The SEM images in **Figure 4.5** (g) and **Figure 4.5** (h) belonging to the electrode obtained at -2.5 V, particularly at 50,000x magnification, display a dense, cauliflower-like morphology. This complex structure results from more vigorous manganese deposition processes occurring at higher voltages. The formation of gas bubbles, likely hydrogen, contributes to the pronounced porosity within the manganese layer. These structural features are significant for enhancing ion transport and energy storage capacity [55], [56]

Comparative Analysis: The bare graphite's innate smoothness contrasts sharply with the textured coatings achieved through manganese electrodeposition. The evolution from a bare to a coated electrode is a testament to the transformative power of electrochemical processes in fabricating advanced materials for energy storage solutions. The deposition of manganese introduces significant morphological changes, transforming the flat layers into a textured surface. As the voltage increases (at negative direction), the effects of electrodeposition compounds move from sparse manganese nucleation sites to a fully developed, complex coating. This evolution not only modifies the surface structure but also enhances the functional characteristics of the electrode, such as increased surface area and porosity, which are critical for energy storage applications.

4.3 XRD Analysis of Flexible Electrodes

The XRD results of uncoated graphite and Mn coated graphite samples are shown **Figure 4.6**. A large peak at around 26.6° and a small peak at around 54.6° are observed for uncoated graphite. These peaks are associated with the graphite peaks corresponding to the (002) and (004) planes presented in the literature [17], [23]. After graphite samples were coated by Mn at various voltages, the intensity of XRD peaks belonging to graphite decreases suggesting a coating on graphite surface. The decrease in peak intensities of the electrodes obtained at -1.5, -2.0, and -2.5 V is proportional to applied growth potential. Upon decreasing growth potential (at more negative potential), the peak intensities of the modified electrodes decreases because the film thickness is higher at the deposition potential of -2.5 V. SEM and XRD have proved that a coating was obtained on graphite surface.

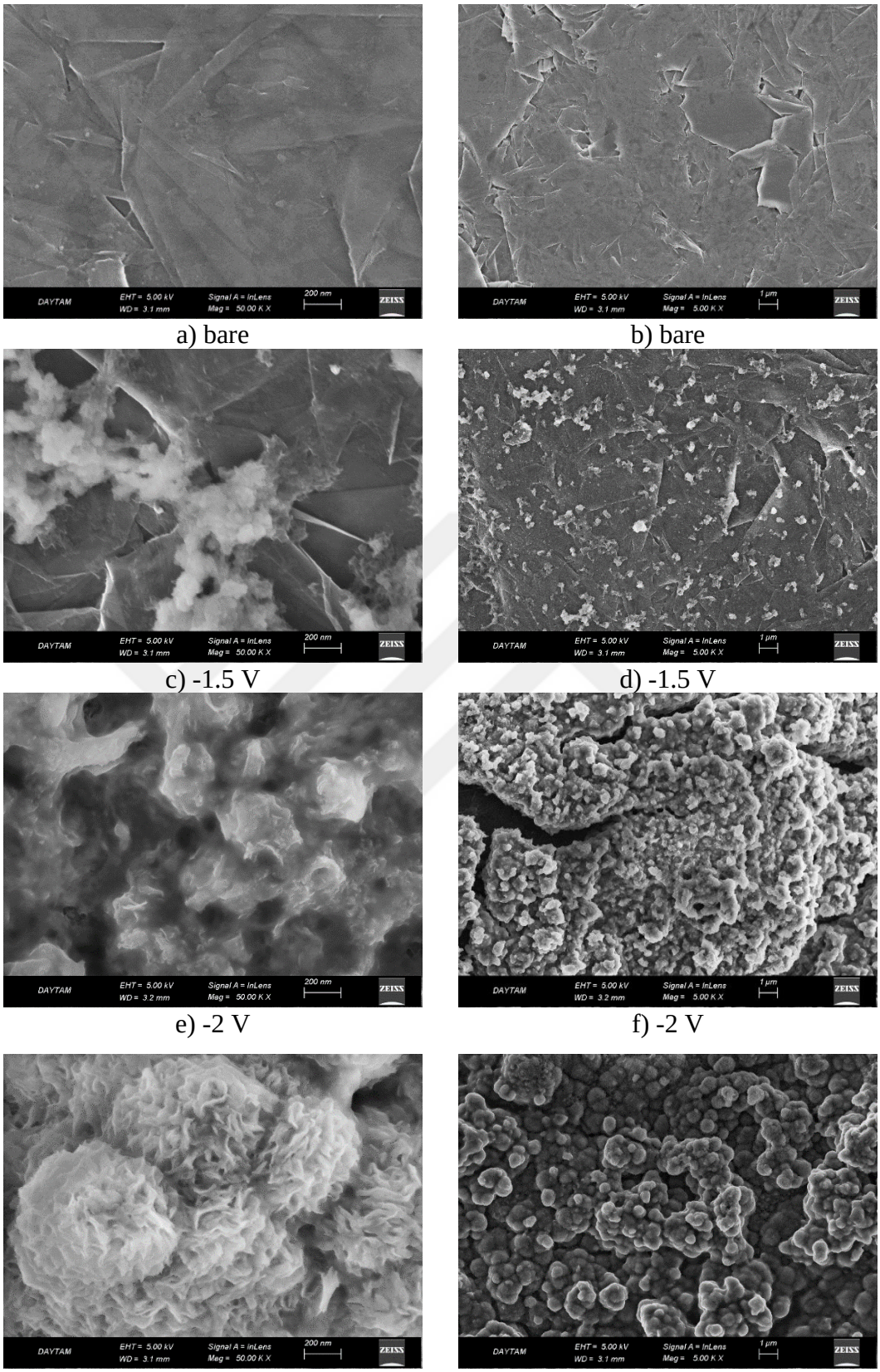

a) bare b) bare

c) -1.5 V d) -1.5 V

e) -2 V f) -2 V

g) -2.5 V h) -2.5 V

Figure 4.5 SEM results for bare and Mn coated graphite tapes. The growth potentials of the film are given under each image.

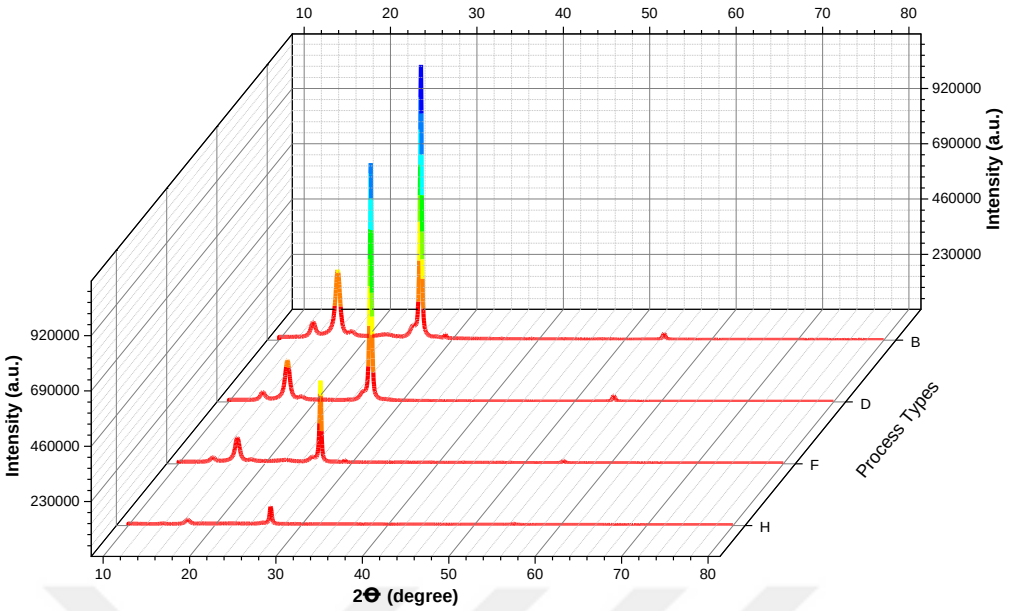

(a)

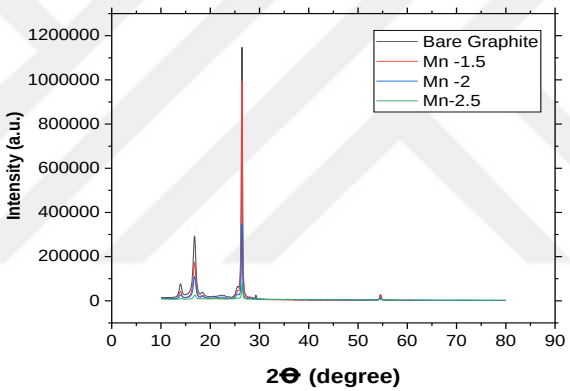

(b)

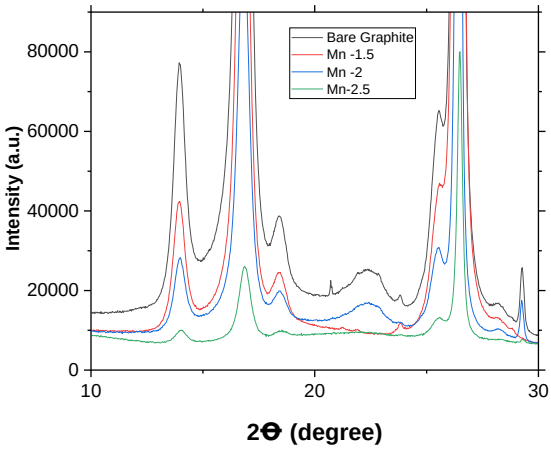

(c)

Figure 4.6 XRD results of bare graphite and Mn coated graphite. The deposition potential of each electrode is presented in the panels.

4.4 FTIR Analysis of Flexible Electrodes

In the Fourier Transform Infrared Spectroscopy (FTIR) in Figure 4.7, the transmittance spectra of bare graphite are compared to those of graphite surfaces coated with manganese (Mn) at electrodeposition voltages of -1.5 V, -2 V, and -2.5 V.

The spectrum for bare graphite, represented by the black line, shows a series of small peaks at wave numbers 3101, 2430, 2160, 2025, 1977, 1684, and 615 cm^{-1}. These peaks are expected due to the stable structure of graphite, which does not usually react in the infrared region. When graphite is coated with Mn by the application of -1.5 V, shown by the red line, new peaks are observed, indicating changes in the surface chemistry. A notable peak is observed around the 1500-1600 cm^{-1} area, which may suggest the formation of manganese oxides. At a higher voltage of -2 V, represented by the blue line, the peaks become clearer and slightly shifted, suggesting a stronger interaction between the manganese and the graphite. This could mean a thicker or more complex layer of manganese oxide is formed.

Finally, at the highest voltage of -2.5 V, shown by the green line, the spectrum displays a significant increase in the clarity and number of peaks, particularly in areas that could be linked to Mn-O bonds. The sharpness of these peaks could indicate a more orderly and denser layer of manganese oxides. The peaks around 3000-3500 cm^{-1} belongs to hydroxide suggesting that Mn could be found as manganese hydroxide.

Overall, the FTIR spectral analysis indicates that the electrodeposition voltage has a notable effect on the manganese oxide/hydroxide development on the graphite surface. The changes in peak intensity and position with different voltages suggest a relationship between the voltage used and the characteristics of the manganese oxide/hydroxide layer that forms, which could impact the material's electrochemical properties.

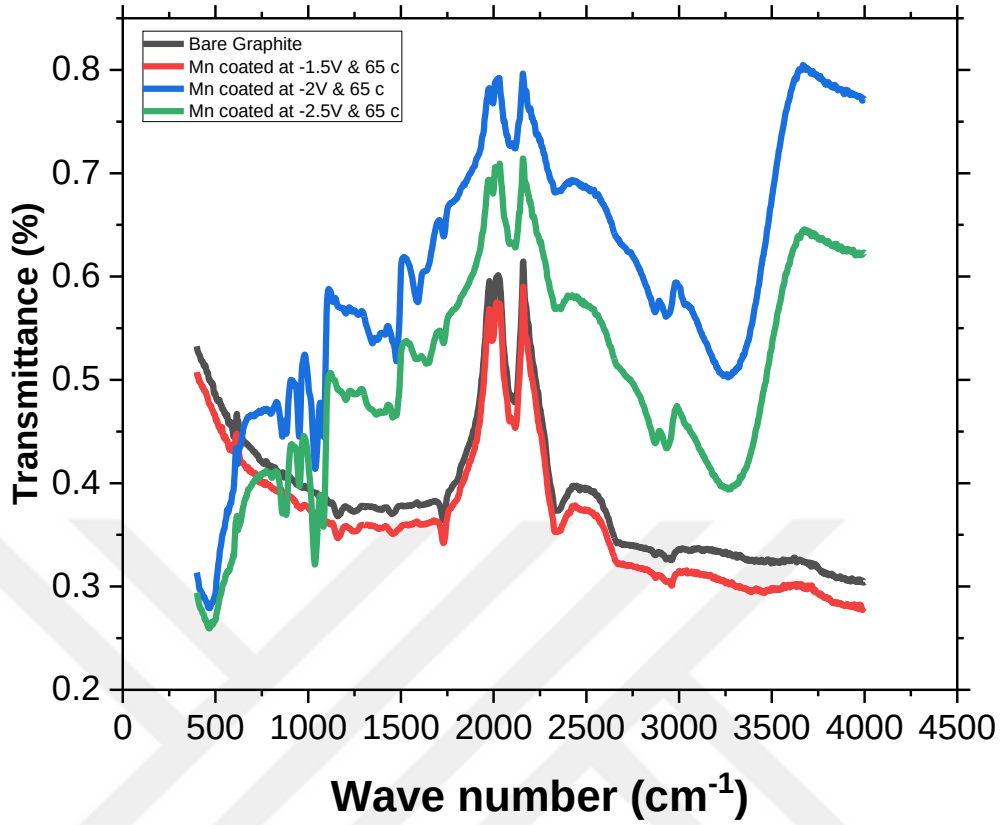

Figure 4.7 FTIR results for bare and Mn coated graphite tapes. The growth potential of the electrode is shown in the panel.

4.5 Fuel Cell Application of The Electrodes

The linear sweep voltammetry of the electrodes was conducted in alkaline solution to test usability of the electrodes for hydrogen evolution reaction (see **Figure 4.8**). Bare and manganese-coated graphite electrodes were scanned in KOH. The current responses of the electrodes electrodeposited by the application of -2.5 V and -2.0 V were close to 0 A. This suggests that these electrodes (obtained by -2.5 V and 2.0 V) cannot cause hydrogen evolution in this electrolyte. The electode formed in a DES by the application of -1.5 V is similar to bare (uncoated) electrode. Therefore, the modified electrodes are **not suitable for fuel cells applications.**

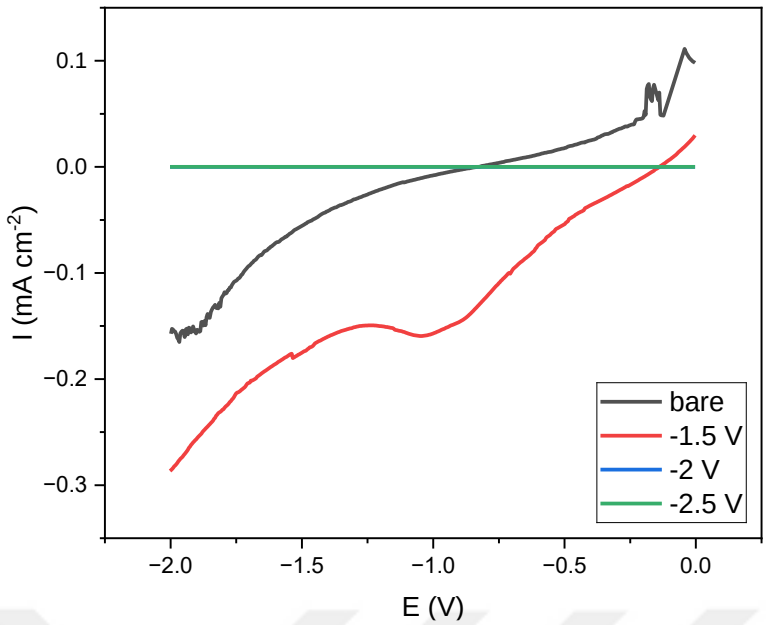

Figure 4.8 Linear Sweep Voltammetry of Bare and Manganese-Coated Graphite in KOH to Evaluate Electrodes Properties for Fuel Cell with Scan Rate of 20 mV s^{-1}

4.6 Cycling of Electrodes in Na_2SO_4 Electrolyte

After coating graphite on tape with Mn-based film, the modified electrodes were transferred to cycling electrolytes. Before electrochemical characterization, the non-electrochemical characterizations of the electrodes were analyzed. The cyclic voltammogram curve for the electrode obtained -1.5 V samples and cycling in aqueous Na_2SO_4 is shown in **Figure 4.9** (a). It reveals a sequence of well-defined redox peaks, indicative of active manganese-based electrode on the graphite surface with aqueous Na_2SO_4 solution. This suggests that as the manganese-based electrode layers rearrange and settle, the surface area available for electrochemical reactions increases, leading to enhanced electrochemical reactivity. Such a pattern of increasing peak prominence corresponds to the activation and surface reorganization phenomena often observed in transitional metal oxide coatings, which are known to improve their electrochemical properties upon initial cycling. Subsequently, the samples were placed in a Na_2SO_4 solution and cycled at a constant scan rate of 50 mV s^{-1}.

The electrode electrodeposited by the application of -1.5 V was first cycled at a wide potential window from -0.8 V to 0.5 V. Later, the same electrode was cycled in the

same electrolyte with narrow potential window from -0.8 V to 0.2 V. The narrow potential window as shown in **Figure 4.9** (b) demonstrates a more restrained cyclic voltammogram's curve with a decreased peak separation, indicating a faster achievement of electrochemical equilibrium. This is typical of electrochemical systems where the reaction space is limited, thereby quickening the redox processes and possibly influencing the rate of charge-discharge cycles in energy storage applications. As narrow potential window could cause more stable behavior in the selected electrolyte, the electrode electrodeposited by the application of -2.0 V was cycled at the potential window from -0.8 V to 0.2 V. The curves belonging to the electrode obtained at -2.0 V is shown in **Figure 4.9** (c) suggesting also more stable electrochemical activities. This could occur due to the growth conditions as more manganese-based film could be electrodeposited on the graphite. The chemical composition (oxide/hydroxide ratio) could contribute to the charge storage mechanism. The cyclic voltammogram curve belonging the electrodes obtained at -2.5 V exhibits sharply defined redox peaks as shown in **Figure 4.9** (d), which are hallmarks of vigorous and stable manganese electrochemical activities. This behavior is indicative of a robust redox process, which could be essential for high-capacity energy storage systems, as it facilitates greater charge storage through efficient electron transfer.

Finaly across the different applied potentials, the manganese-coated graphite electrodes demonstrate capacitive characteristics that are fundamental to the operation of supercapacitors. The cyclic voltammogram profiles provide valuable insights into the electrochemical stability and reversibility of the oxidation and reduction reactions of manganese-based electrode. The comparative analysis suggests that while all potentials facilitate capacitive behavior, a wider potential window, as seen for the electrode grown by the application of -2.5 V, may be more conducive to achieving superior supercapacitor performance due to higher charge, the enhanced stability and comprehensive electrochemical activity it provides.[57], [58]

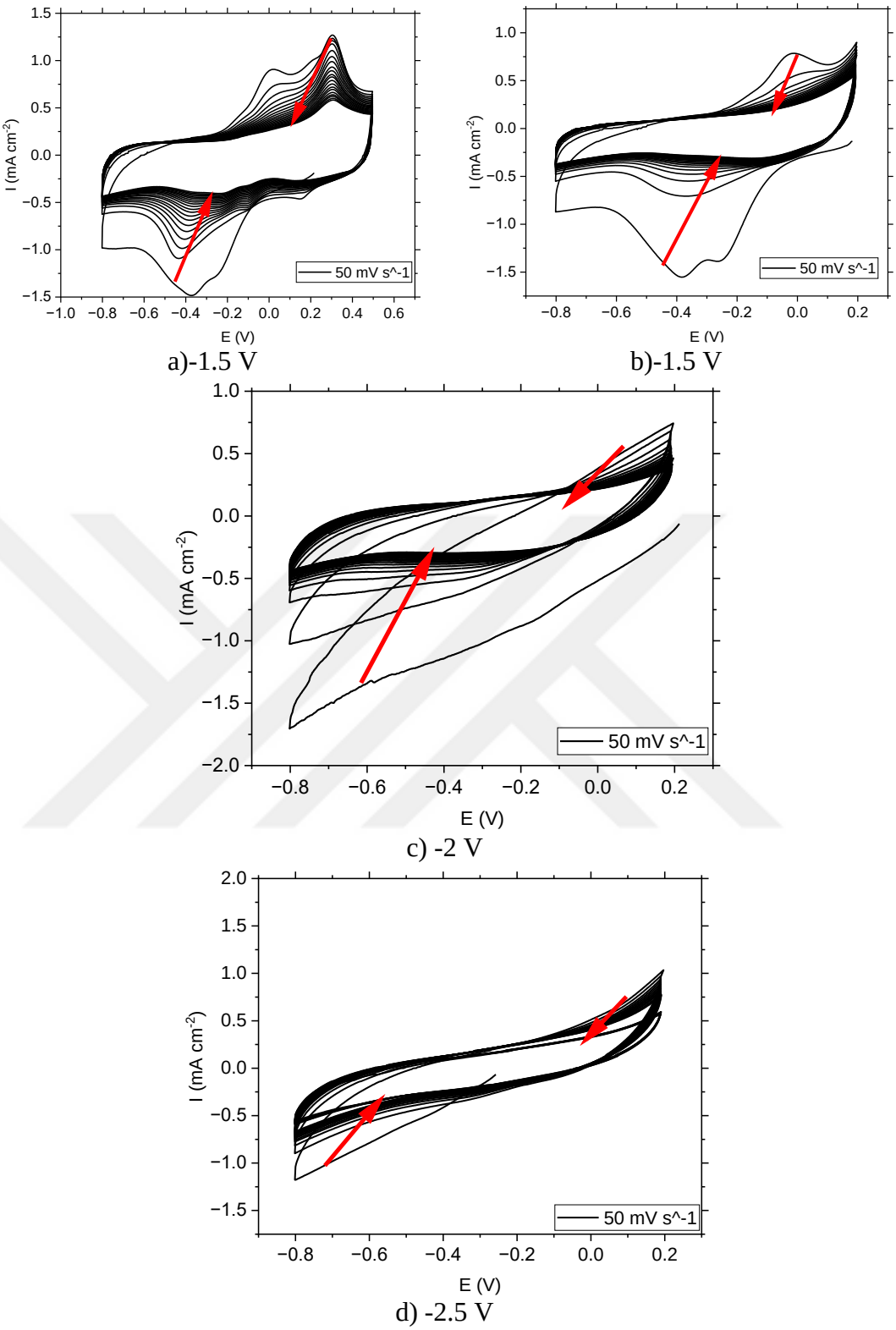

Figure 4.9 Cyclic voltammogram data cycled in Na_2SO_4. The cycling electrodes were electrodeposited when the growth potential was -1.5 V and cycling potential window a) between -0.8 and 0.5 V; b) between -0.8 and 0.2 V. Cyclic voltammogram data cycled in Na_2SO_4. The cycling electrodes were electrodeposited when the growth potential was c) -2.0 V and; d) -2.5 V.

4.7 Analysis of the Electrodes in Na_2SO_4 with Different Scan Rates

Mn-based film on graphite was cycled in Na_2SO_4 solution and the resulting cyclic voltammogram data for the same scan rate were presented in the previous section. The same film was cycled in the same electrolyte (Na_2SO_4 bath) with different scan rates. The cyclic voltammetry analysis presented here provides a detailed examination of the electrochemical characteristics of manganese-based coated graphite electrodes, where the coating process was conducted at different applied potentials of -1.5 V, -2 V, and -2.5 V. **Figure 4.10** displays cyclic voltammogram curves at various scan rates in Na_2SO_4 solution, offering insights into the capacitance results.

For the electrodes coated at -1.5 V **Figure 4.10** (a), an increase in the scan rate from 10 mV/s to 100 mV/s results in a noticeable broadening of the cyclic voltammogram curves, indicative of faster electron transfer processes at higher scan rates. This aligns with kinetic-controlled reactions where mass transport to the electrode surface becomes slower [59].

For electrodes coated at -2 V **Figure 4.10** (b), the cyclic voltammogram curves show a broadening effect with increasing scan rates, with more pronounced peaks compared to those coated at -1.5 V. This suggests enhanced electrochemical activity for the manganese-based coating on graphite electrodes at -2 V, possibly due to a higher degree of manganese deposition or altered surface properties [60].

The cyclic voltammogram curves of the electrode coated at -2.5 V **Figure 4.10** (c) exhibit even more pronounced peaks at higher scan rates, indicating a highly active electrode surface. The increased peak current with higher scan rates suggests kinetic-controlled electrode processes occurring over an expanded active surface area or involving a greater number of electroactive sites. SEM images confirm that the thickness of the -2.5 V sample has a more extensive active area and could be resulting in higher specific capacitance [61].

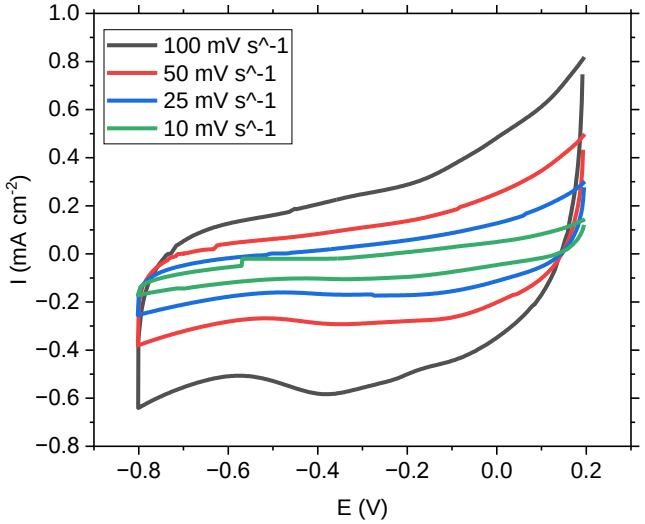

a)-1.5 V sample

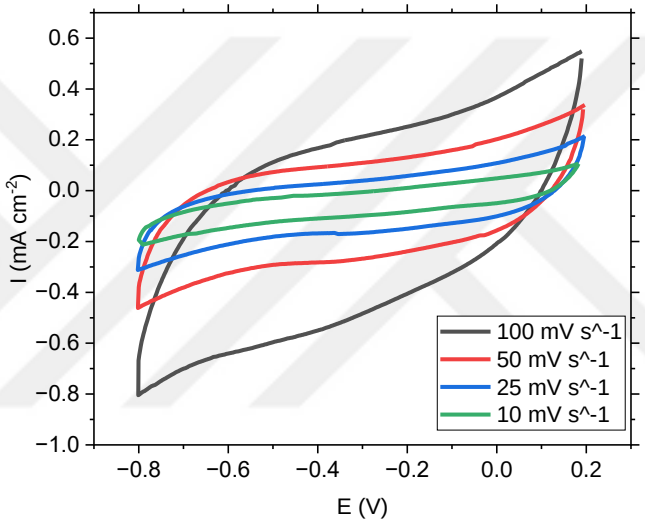

b) -2 V sample

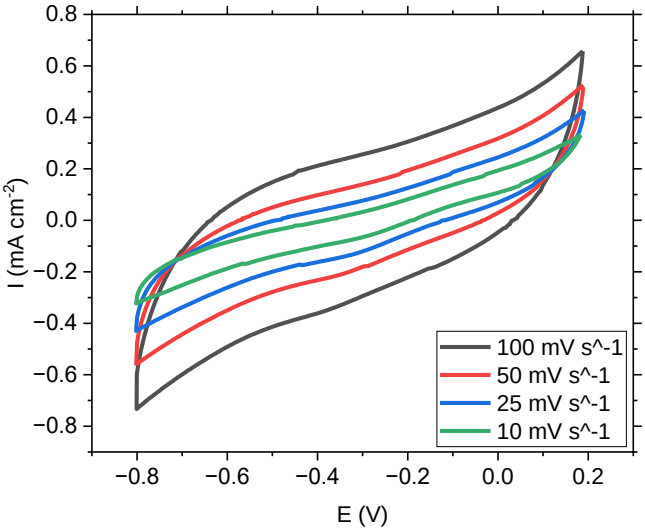

c) -2.5 V sample

Figure 4.10 a) Cyclic voltammogram data cycled in Na_2SO_4. The cycling electrodes were electrodeposited when the growth potential was a) -1.5 V b) -2.0 V and; c) -2.5 V. The scan rates are indicated in the panels.

4.8 Cycling of Electrodes in KOH Electrolyte

In the comparison of the three diagrams in the **Figure 4.11**, where -1.5 V, -2 V, and -2.5 V are the potentials at which manganese was deposited on graphite tapes within an Ethaline DES for 500 seconds at a temperature of 60°C, significant differences in the cycling behavior were observed. Subsequently, the samples were placed in a potassium hydroxide (KOH) solution at a constant scan rate of 50 mV s^{-1}.

The electrode electrodeposited by the application of -1.5 V was first cycled at a potential window from -0.8 V to 0.2 V in alkaline solution as the same electrode was cycled in neutral solution. The manganese deposition on graphite tapes was gradual and controlled, reaching a state of stability more swiftly. The cyclic voltammogram of the electrode cycling in KOH electrolyte is stable.

The electrode electrodeposited by the application of -2.0 V was cycled at the same potential window from -0.8 V to 0.2 V. A sharper ascent in current density was observed, reflecting a more stable manganese deposition process. This indicated a more dynamic process, where the increased potential drove quicker layering but also necessitated an extended period for the reaction to achieve stability.

The cyclic voltammogram curve belonging the electrodes obtained at -2.5 V exhibits sharply defined redox peaks. The most aggressive deposition was observed, with the highest current density peaks.

When cycled in the KOH solution, the impact of the initial deposition potential became evident, with the higher potentials showing more pronounced electrochemical activity in the KOH environment. This comparison across the three applied potentials demonstrated a clear relationship between the deposition potential and the stabilization time, with higher potentials leading to increased rates of manganese deposition but also requiring longer times to achieve electrochemical stability.

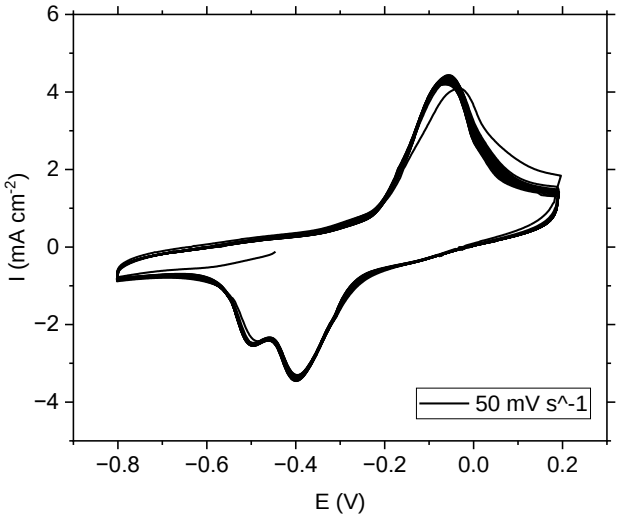

a) -1.5 V

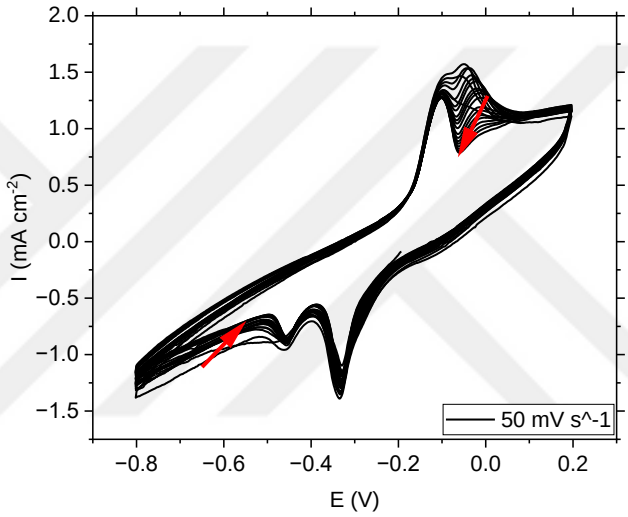

b) -2 V

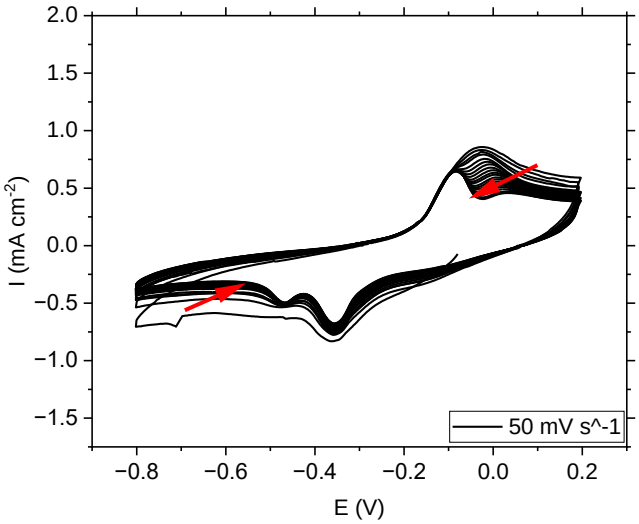

c) -2.5 V

Figure 4.11 a) Cyclic voltammogram data cycled in KOH. The cycling electrodes were electrodeposited when the growth potential was a) -1.5 V b) -2.0 V and; c) -2.5 V. The scan rates are indicated in the panels.

4.9 Analysis of the Electrodes in KOH with Different Scan Rate

The coating of manganese onto graphite tapes was obtained under the application of varying potentials: -1.5 V, -2 V, and -2.5 V, within an Ethaline-based Deep Eutectic Solvent (DES) at the temperature of 60°C over a period of 500 seconds. The resultant samples were then analyzed using cyclic voltammetry at different scan rates to ascertain the electrochemical behavior post-coating. For the samples coated at -1.5 V as depicted in Figure 4.12(a), a widening of the CYCLIC VOLTAMMOGRAM curves was observed with increasing scan rates from 10 mV/s to 100 mV/s. This widening is indicative of a uniform and controlled electron transfer process, which is characteristic of diffusion-like reactions, signifying a consistent manganese deposition across the graphite surface. At the coating potential of -2 V as shown in Figure 4.12(b), an increase in electrochemical activity was noted. The cyclic voltammogram curves broadened more prominently with increasing scan rates, suggesting an accelerated rate of manganese deposition, which likely led to a moderately increased thickness of the manganese layer compared to the electrode deposited at -1.5 V in Ethaline environment having Mn^{2+} ions. The most substantial changes were noted at the electrode grown at -2.5 V coating potential as observed in Figure 4.12(c), where the cyclic voltammogram curves revealed markedly pronounced peaks at higher scan rates, indicating a highly active electrode surface. Such increased activity can be attributed to a thicker manganese coating, which was corroborated by SEM analysis. The thicker layer normally could achieve a larger active surface area, contributing to enhanced charge transfer and a higher specific capacitance. However, this is not the case in these results because KOH ions could not react highly with the electrode electrodeposited by -2.5 V. It is evident that the electrodeposition potential significantly influences the manganese coating's thickness and the resultant electrochemical behavior of the electrodes. As the electrodeposition potential was varied from -1.5 V to -2.5 V, there was a clear impact on the morphology and electrochemical properties of the manganese-coated graphite electrodes. The coating thickness increased with higher deposition potentials (more negative potential), leading to a lower electroactive surface coverage because the electrode obtained by the application of -1.5 V showed higher current density than other electrodes. Ions in cycling electrolytes could have higher flux when the substrate has thinner film causing less agglomerated particles. The enhanced electrochemical reactivity, particularly at the -1.5 V potential, demonstrated the low coating thickness however high electrochemical activity. This underlines the importance of carefully selecting the electrodeposition conditions to tailor the electrode's performance for specific applications.

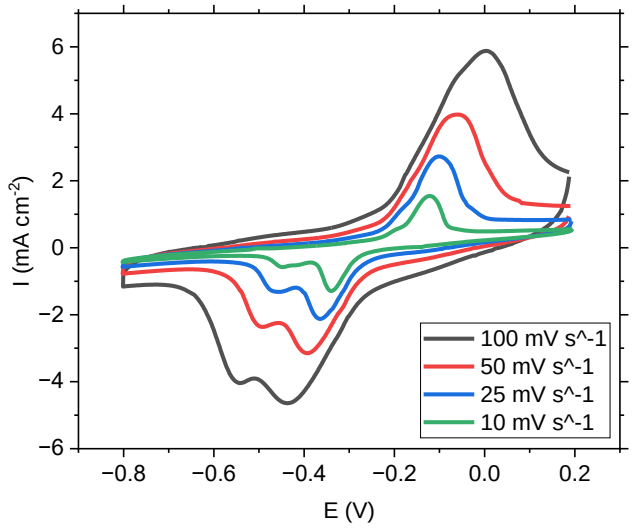

a) -1.5 V sample

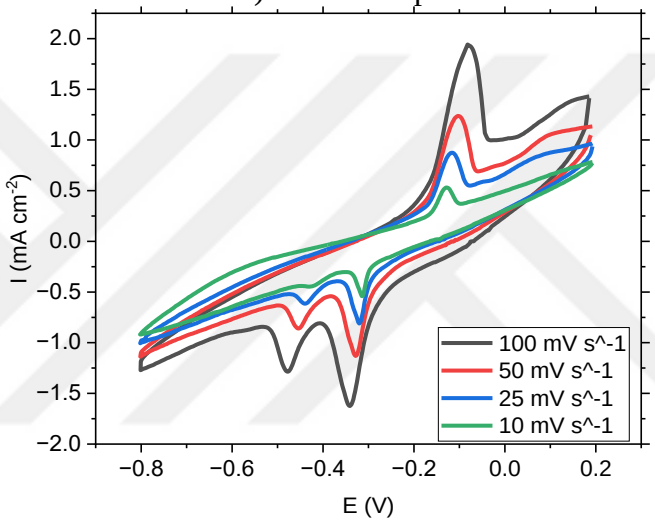

b) -2 V sample

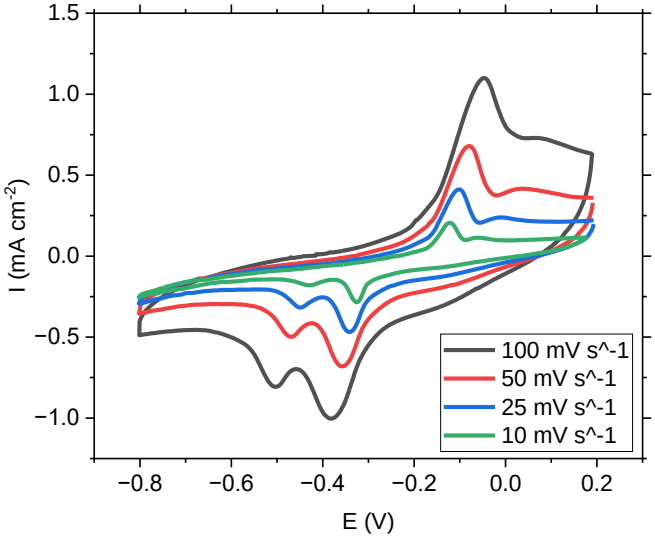

c) -2.5 V sample

Figure 4.12 a) Cyclic voltammogram data cycled in KOH. The cycling electrodes were electrodeposited when the growth potential was a) -1.5 V b) 2.0 V and; c) -2.5 V. The scan rates are indicated in the panels.

4.10 Comparation Specific Capacitance of Electrodes in KOH and Na_2SO_4

Upon rigorous examination of the experimental data, it was discerned that the specific capacitance of manganese-based coating electrodes exhibited a propensity to diminish with increasing scan rates. This trend was consistently observed across electrolytes of Na_2SO_4 and KOH. A plausible explanation for this phenomenon is surmised to be the limited ion migration time to the electrode's surface at escalated scan rates, which in turn, adversely affects the electrical storage efficiency. The specific capacitance (C_s) of the electrodes was calculated by the Equation [62]

$$C_s = \frac{\int I.dV}{A.v.\Delta V} \quad (4.1)$$

In which $I.dV$ is the area under the cyclic voltammogram curve, A express area of the electrode, v emphasize scan rate and ΔV illustrates potential window. The specific capacitance of the electrodes electrodeposited by various potential and cycled in different electrolytes is presented.

Table 4.1 Specific capacitance values of Mn coated graphite tapes obtained at -1.5 V potential depending on the varying scanning rates in different electrolyte solutions

Scan Rate ($mV\ s^{-1}$)	Specific Capacitance ($mF\ cm^{-2}$) in Na_2SO_4	Specific Capacitance ($mF\ cm^{-2}$) in KOH
100	7.14	32.62
50	7.47	35.75
25	7.80	38.47
10	8.36	40.20

Table 4.2 Specific capacitance values of Mn coated graphite tapes obtained at -2 V potential depending on the varying scanning rates in different electrolyte solutions

Scan Rate ($mV\ s^{-1}$)	Specific Capacitance ($mF\ cm^{-2}$) in Na_2SO_4	Specific Capacitance ($mF\ cm^{-2}$) in KOH
100	5.78	7.16
50	6.65	9.10
25	7.50	13.32
10	8.76	25.76

Table 4.3 Specific capacitance values of Mn coated graphite tapes obtained at -2.5 V potential depending on the varying scanning rates in different electrolyte solutions

Scan Rate ($mV\ s^{-1}$)	**Specific Capacitance ($mF\ cm^{-2}$) in Na_2SO_4**	**Specific Capacitance ($mF\ cm^{-2}$) in KOH**
100	4.80	6.38
50	5.78	7.28
25	7.02	8.17
10	8.71	8.88

Remarkably, electrodes coated at an elevated potential of -2.5 V demonstrated similar specific capacitance in comparison to those coated at -1.5 V and -2 V when the electrolyte is neutral, and the scan rate is low. It is postulated that the increased electrodeposition potential causes a more compact manganese deposition, thereby the effective surface area available for charge accumulation is low, as illustrated by the lower capacitance values, particularly notable at the 100 mV/s scan rate in the KOH medium.

The influence of the electrolytic medium on the specific capacitance was also substantiated, with the KOH medium outperforming Na_2SO_4. This assertion has been supported by the current density values observed in the KOH medium, which remained significantly higher across all scan rates.

These findings underscore the imperative of optimizing electrodeposition potential, scan rate, and electrolyte selection to enhance the electrodes' performance for energy storage applications. The data delineate the delicate balance required to refine the electrochemical characteristics of materials, vital for the advancement of high-capacity energy storage systems.

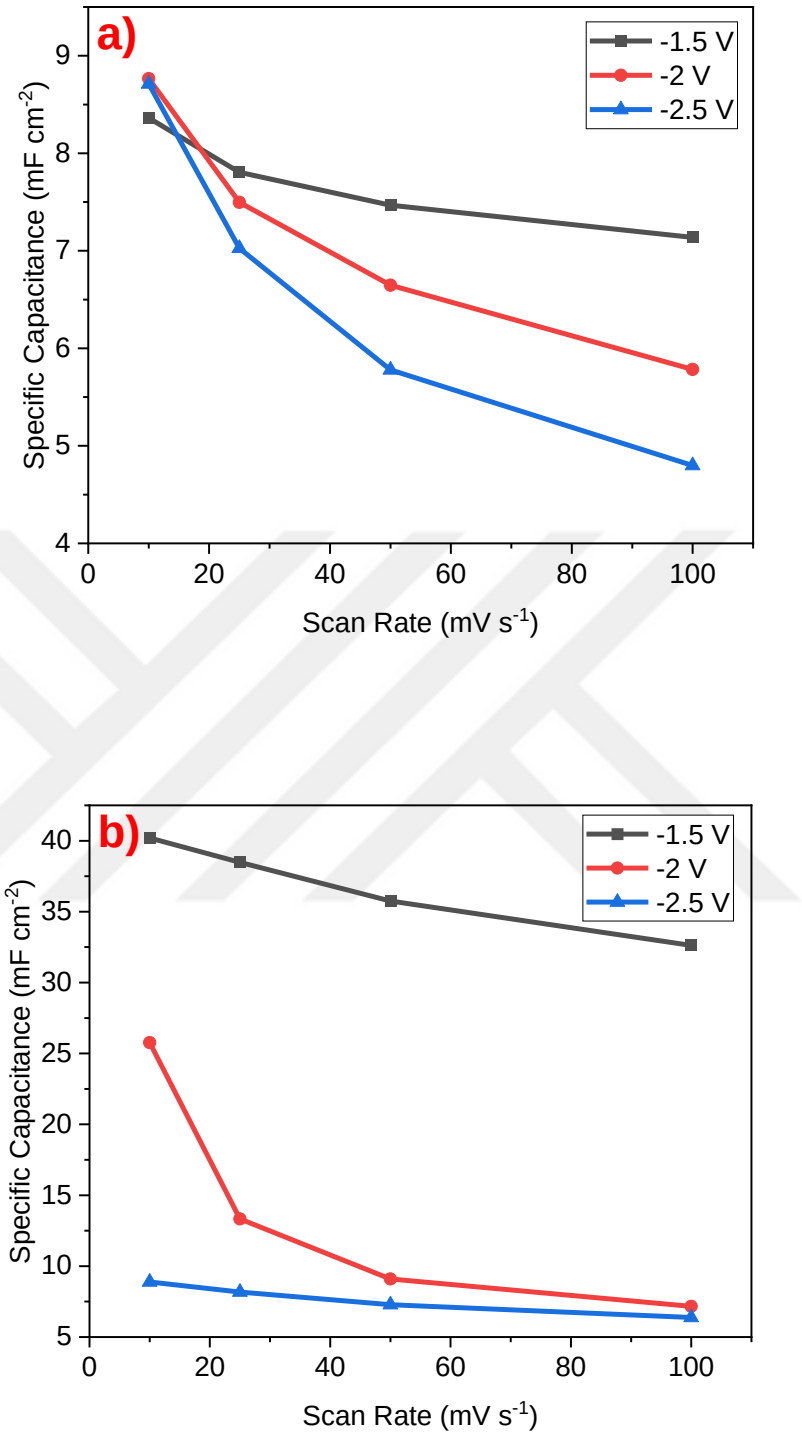

Figure 4.13 specific capacitance of the modified electrodes cycled in a) Na_2SO_4 and b) KOH electrolyte.

CHAPTER 5
CONCLUSION

In the realm of flexible electronics, the advancement of flexible electrode technology has not kept pace with the rapid development observed in flexible screens. This study delves into the potential application of flexible electrodes, both as energy storage materials and as fuel cells in wearable electronics. Recognizing the necessity for pliable substrates, or current collectors, for these modified electrodes, this research has utilized graphite coated tape as the substrate. The primary focus has been on the development of an economical and efficient flexible electrode for energy storage and conversion applications, aiming to overcome the cost barriers associated with existing flexible electrodes. Central to this study is the electrodeposition of manganese onto graphite substrates within deep eutectic solvent (DES) electrolytes. For this purpose, 0.1 M $MnCl_2$ was dissolved in Ethaline solutions, and manganese was electrodeposited onto the substrates at various potentials (-1.5 V, -2.0 V, and -2.5 V) for a duration of 500 seconds. The resulting modified electrodes underwent thorough characterization using X-ray diffraction (XRD), Fourier transform infrared spectroscopy (FTIR), and scanning electron microscopy (SEM), revealing their structural and spectroscopic properties. Furthermore, the electrochemical behavior of both the unmodified graphite and the manganese-modified electrodes was meticulously analyzed through cyclic voltammetry. One of the critical phases of this research involved cycling the electrodes in 1 M KOH and 1 M Na_2SO_4 electrolytes to determine their specific capacitance and to evaluate the influence of different deposition potentials on their performance. The manganese coated electrodes could not be suitable for hydrogen evolution reaction in alkaline solution and cannot be used in fuel cell application. A notable finding was that lower, more negative deposition voltages led to the formation of denser manganese-based layers, while higher potential resulted in thinner films. Intriguingly, these thinner films exhibited enhanced specific capacitance, likely due to increased ion flux on the coating. This study thereby demonstrates the practicality of using manganese-coated graphite flexible electrodes in both alkaline and neutral media for flexible energy storage devices. It highlights the potential of these electrodes to provide cost-effective,

efficient, and adaptable solutions for the next generation of flexible energy storage technologies.

This comprehensive approach to developing flexible electrodes presents a significant advancement in the field, particularly in addressing the challenges of cost and performance. By optimizing the electrodeposition conditions and thoroughly analyzing the electrochemical and structural properties of the modified electrodes, this research contributes valuable insights into the design and application of flexible energy storage systems. The successful implementation of manganese-coated graphite electrodes in diverse media underscores their versatility and potential as a key component in the evolving landscape of wearable electronics and energy storage solutions.

REFERENCES

[1] A. Yavuz, M. Bedir, and A. Tunç, "Manganese – iron coated flexible graphite sheet having wide potential window for energy storage devices," *J Energy Storage*, vol. 50, p. 104253, Jun. 2022, doi: 10.1016/J.EST.2022.104253.

[2] A. Yavuz, N. Ozdemir, P. Yilmaz Erdogan, H. Zengin, G. Zengin, and M. Bedir, "Effect of electrodeposition potential and time for nickel film generation from ionic liquid electrolytes for asymmetric supercapacitor production," *Thin Solid Films*, vol. 711, Oct. 2020, doi: 10.1016/j.tsf.2020.138309.

[3] A. Yavuz, P. Yilmaz Erdogan, N. Ozdemir, H. Zengin, G. Zengin, and M. Bedir, "Effect of cathodic deposition potential on the performance of nanostructured cobalt-based film for asymmetric supercapacitor fabrication," *Solid State Sci*, vol. 99, Jan. 2020, doi: 10.1016/j.solidstatesciences.2019.106074.

[4] S. Wustoni, G. Nikiforidis, S. Inal, Y. S. Indartono, V. Suendo, and B. Yuliarto, "Hydroxymethyl PEDOT microstructure-based electrodes for high-performance supercapacitors," *APL Mater*, vol. 10, no. 6, Jun. 2022, doi: 10.1063/5.0088452.

[5] S. G. Anton and A. E. Afloarei Nucu, "The effect of financial development on renewable energy consumption. A panel data approach," *Renew Energy*, vol. 147, pp. 330–338, Mar. 2020, doi: 10.1016/j.renene.2019.09.005.

[6] S. Koohi-Fayegh and M. A. Rosen, "A review of energy storage types, applications and recent developments," *Journal of Energy Storage*, vol. 27. Elsevier Ltd, Feb. 01, 2020. doi: 10.1016/j.est.2019.101047.

[7] R. Liu, M. Liu, Y. Zhao, Y. Ma, and J. Yan, "Thermodynamic study of a novel lignite poly-generation system driven by solar energy," *Energy*, vol. 214, Jan. 2021, doi: 10.1016/j.energy.2020.119075.

[8] A. Rimpel *et al.*, “Mechanical energy storage,” *Thermal, Mechanical, and Hybrid Chemical Energy Storage Systems*, pp. 139–247, Jan. 2021, doi: 10.1016/B978-0-12-819892-6.00004-6.

[9] S. A. Qadir, H. Al-Motairi, F. Tahir, and L. Al-Fagih, “Incentives and strategies for financing the renewable energy transition: A review,” *Energy Reports*, vol. 7. Elsevier Ltd, pp. 3590–3606, Nov. 01, 2021. doi: 10.1016/j.egyr.2021.06.041.

[10] D. M. Gioutsos, K. Blok, L. van Velzen, and S. Moorman, “Cost-optimal electricity systems with increasing renewable energy penetration for islands across the globe,” *Appl Energy*, vol. 226, pp. 437–449, Sep. 2018, doi: 10.1016/j.apenergy.2018.05.108.

[11] S. Ould Amrouche, D. Rekioua, T. Rekioua, and S. Bacha, “Overview of energy storage in renewable energy systems,” *Int J Hydrogen Energy*, vol. 41, no. 45, pp. 20914–20927, Dec. 2016, doi: 10.1016/j.ijhydene.2016.06.243.

[12] I. Hadjipaschalis, A. Poullikkas, and V. Efthimiou, “Overview of current and future energy storage technologies for electric power applications,” *Renewable and Sustainable Energy Reviews*, vol. 13, no. 6–7. pp. 1513–1522, Aug. 2009. doi: 10.1016/j.rser.2008.09.028.

[13] J. Zhang, L. Zhang, F. Sun, and Z. Wang, “An Overview on Thermal Safety Issues of Lithium-ion Batteries for Electric Vehicle Application,” *IEEE Access*, vol. 6, pp. 23848–23863, May 2018, doi: 10.1109/ACCESS.2018.2824838.

[14] H. Kamberaj, “Capacitance and Dielectrics,” in *Electromagnetism: With Solved Problems*, H. Kamberaj, Ed., Cham: Springer International Publishing, 2022, pp. 77–107. doi: 10.1007/978-3-030-96780-2_4.

[15] V. S. Marin Halper James C Ellenbogen, “Supercapacitors: A Brief Overview MITRE MITRE MITRE MITRE,” 2006. [Online]. Available: http://www.mitre.org/tech/nanotech

[16] T. Selvaraj, V. Perumal, S. F. Khor, L. S. Anthony, S. C. B. Gopinath, and N. Muti Mohamed, “The recent development of polysaccharides biomaterials and their

performance for supercapacitor applications," *Materials Research Bulletin*, vol. 126. Elsevier Ltd, Jun. 01, 2020. doi: 10.1016/j.materresbull.2020.110839.

[17] F. Yu, T. Wang, Z. Wen, and H. Wang, "High performance all-solid-state symmetric supercapacitor based on porous carbon made from a metal-organic framework compound," *J Power Sources*, vol. 364, pp. 9–15, 2017, doi: 10.1016/j.jpowsour.2017.08.013.

[18] J. Tahalyani, M. J. Akhtar, J. Cherusseri, and K. K. Kar, "Characteristics of Capacitor: Fundamental Aspects," in *Handbook of Nanocomposite Supercapacitor Materials I: Characteristics*, K. K. Kar, Ed., Cham: Springer International Publishing, 2020, pp. 1–51. doi: 10.1007/978-3-030-43009-2_1.

[19] K. Urita, C. Urita, K. Fujita, K. Horio, M. Yoshida, and I. Moriguchi, "The ideal porous structure of EDLC carbon electrodes with extremely high capacitance," *Nanoscale*, vol. 9, no. 40, pp. 15643–15649, 2017, doi: 10.1039/C7NR05307J.

[20] J. R. Miller, "Perspective on electrochemical capacitor energy storage," *Appl Surf Sci*, vol. 460, pp. 3–7, Dec. 2018, doi: 10.1016/j.apsusc.2017.10.018.

[21] N. Omar, J. Van Mierlo, B. Verbrugge, and P. Van Den Bossche, "Power and life enhancement of battery-electrical double layer capacitor for hybrid electric and charge-depleting plug-in vehicle applications," in *Electrochimica Acta*, Oct. 2010, pp. 7524–7531. doi: 10.1016/j.electacta.2010.03.039.

[22] P. Simon, Y. Gogotsi, and B. Dunn, "Where Do Batteries End and Supercapacitors Begin?," *Science (1979)*, vol. 343, no. 6176, pp. 1210–1211, Mar. 2014, doi: 10.1126/science.1249625.

[23] L. Zhou, C. Li, X. Liu, Y. Zhu, Y. Wu, and T. van Ree, "Metal oxides in supercapacitors," in *Metal Oxides in Energy Technologies*, Elsevier, 2018, pp. 169–203. doi: 10.1016/b978-0-12-811167-3.00007-9.

[24] D. Majumdar, M. Mandal, and S. K. Bhattacharya, "Journey from supercapacitors to supercapatteries: recent advancements in electrochemical energy storage systems", doi: 10.1007/s42247-020-00090-5/Published.

[25] Z. S. Iro, C. Subramani, and S. S. Dash, “A brief review on electrode materials for supercapacitor,” *International Journal of Electrochemical Science*, vol. 11, no. 12. Electrochemical Science Group, pp. 10628–10643, 2016. doi: 10.20964/2016.12.50.

[26] Y. Wang, J. Guo, T. Wang, J. Shao, D. Wang, and Y. W. Yang, “Mesoporous transition metal oxides for supercapacitors,” *Nanomaterials*, vol. 5, no. 4. MDPI AG, pp. 1667–1689, Oct. 14, 2015. doi: 10.3390/nano5041667.

[27] J. Yan, Q. Wang, T. Wei, and Z. Fan, “Recent advances in design and fabrication of electrochemical supercapacitors with high energy densities,” *Adv Energy Mater*, vol. 4, no. 4, Mar. 2014, doi: 10.1002/aenm.201300816.

[28] A. Muzaffar, M. B. Ahamed, K. Deshmukh, and J. Thirumalai, “A review on recent advances in hybrid supercapacitors: Design, fabrication and applications,” *Renewable and Sustainable Energy Reviews*, vol. 101. Elsevier Ltd, pp. 123–145, Mar. 01, 2019. doi: 10.1016/j.rser.2018.10.026.

[29] O. Z. Sharaf and M. F. Orhan, “An overview of fuel cell technology: Fundamentals and applications,” *Renewable and Sustainable Energy Reviews*, vol. 32. pp. 810–853, Apr. 2014. doi: 10.1016/j.rser.2014.01.012.

[30] N. Sankararamakrishnan, P. Kumar, and V. Singh Chauhan, “Modeling fixed bed column for cadmium removal from electroplating wastewater,” *Sep Purif Technol*, vol. 63, no. 1, pp. 213–219, Oct. 2008, doi: 10.1016/j.seppur.2008.05.002.

[31] J. Costard, M. Ender, M. Weiss, and E. Ivers-Tiffée, “Three-Electrode Setups for Lithium-Ion Batteries,” *J Electrochem Soc*, vol. 164, no. 2, pp. A80–A87, 2017, doi: 10.1149/2.0241702jes.

[32] S. Holla and M. Selvakumar, “Effect of Different Electrolytes on the Supercapacitor Behavior of Single and Multilayered Electrode Materials Based on Multiwalled Carbon Nanotube/Polyaniline Composite,” *Macromol Chem Phys*, vol. 219, no. 21, Nov. 2018, doi: 10.1002/macp.201800213.

[33] N. A. Samsudin *et al.*, “Titanium Dioxide Nanostructured Based Supercapacitors,” *Encyclopedia of Energy Storage: Volume 1-4*, vol. 1–4, pp. 361–373, Jan. 2022, doi: 10.1016/B978-0-12-819723-3.00030-5.

[34] M. M. Amaral, R. Venâncio, A. C. Peterlevitz, and H. Zanin, “Recent advances on quasi-solid-state electrolytes for supercapacitors,” *Journal of Energy Chemistry*, vol. 67, pp. 697–717, Apr. 2022, doi: 10.1016/J.JECHEM.2021.11.010.

[35] A. Cuesta, J. Cheng, and E. Herrero, “Electrochemistry in non-conventional electrolytes,” *Electrochemical Science Advances*, vol. 3, no. 4. John Wiley and Sons Inc, Aug. 01, 2023. doi: 10.1002/elsa.202300020.

[36] R. Horia, D.-T. Nguyen, A. Yong, S. Eng, and Z. W. Seh, “Comparative Study of Conventional Electrolytes for Rechargeable Magnesium Batteries.”

[37] G. Oltean *et al.*, “Towards li-ion batteries operating at 80°C: Ionic liquid versus conventional liquid electrolytes,” *Batteries*, vol. 4, no. 1, Mar. 2018, doi: 10.3390/batteries4010002.

[38] C. Austen Angell, Y. Ansari, and Z. Zhao, “Ionic Liquids: Past, present and future,” *Faraday Discussions*, vol. 154. pp. 9–27, 2012. doi: 10.1039/c1fd00112d.

[39] A. Noda and M. Watanabe, “Highly conductive polymer electrolytes prepared by in situ polymerization of vinyl monomers in room temperature molten salts,” 2000. [Online]. Available: www.elsevier.nl/locate/electacta

[40] X. Li, Y. Zheng, and C. Y. Li, “Dendrite-free, wide temperature range lithium metal batteries enabled by hybrid network ionic liquids,” *Energy Storage Mater*, vol. 29, pp. 273–280, Aug. 2020, doi: 10.1016/j.ensm.2020.04.037.

[41] S. Pandey, “Analytical applications of room-temperature ionic liquids: A review of recent efforts,” *Analytica Chimica Acta*, vol. 556, no. 1. pp. 38–45, Jan. 18, 2006. doi: 10.1016/j.aca.2005.06.038.

[42] M. Jafari, S. Z. Shafaie, H. Abdollahi, and A. Entezari-Zarandi, “A Green Approach for Selective Ionometallurgical Separation of Lithium from Spent Li-Ion Batteries by Deep Eutectic Solvent (DES): Process Optimization and Kinetics Modeling,”

Mineral Processing and Extractive Metallurgy Review, vol. 44, no. 3, pp. 218–230, 2023, doi: 10.1080/08827508.2022.2042282.

[43] A. A. Bunaciu, E. gabriela Udriştioiu, and H. Y. Aboul-Enein, "X-Ray Diffraction: Instrumentation and Applications," *Critical Reviews in Analytical Chemistry*, vol. 45, no. 4. Taylor and Francis Ltd., pp. 289–299, Oct. 02, 2015. doi: 10.1080/10408347.2014.949616.

[44] X. Lu, K. Shih, X. Y. Li, G. Liu, E. Y. Zeng, and F. Wang, "Accuracy and application of quantitative X-ray diffraction on the precipitation of struvite product," *Water Res*, vol. 90, pp. 9–14, Mar. 2016, doi: 10.1016/j.watres.2015.12.014.

[45] A. Fadlelmoula, D. Pinho, V. H. Carvalho, S. O. Catarino, and G. Minas, "Fourier Transform Infrared (FTIR) Spectroscopy to Analyse Human Blood over the Last 20 Years: A Review towards Lab-on-a-Chip Devices," *Micromachines*, vol. 13, no. 2. MDPI, Feb. 01, 2022. doi: 10.3390/mi13020187.

[46] R. Heard, J. E. Huber, C. Siviour, G. Edwards, E. Williamson-Brown, and K. Dragnevski, "An investigation into experimental in situ scanning electron microscope (SEM) imaging at high temperature," *Review of Scientific Instruments*, vol. 91, no. 6, p. 063702, Jun. 2020, doi: 10.1063/1.5144981.

[47] B. Rajini, A. V. Narasimha Rao, and C. Sashidhar, "Micro-level studies of fly ash and GGBS—based geopolymer concrete using SEM and XRD," *IOP Conf Ser Mater Sci Eng*, vol. 1130, no. 1, p. 012062, Apr. 2021, doi: 10.1088/1757-899x/1130/1/012062.

[48] J.-S. Yu and Z.-X. Zhang, "Double potential-step chronoamperometry and chronocoulometry at an ultramicrodisk electrode: Theory and experiment 1," 1997.

[49] M. Gulppi, J. P. Irrazabal, M. I. Azócar, F. Scholz, and M. Páez, "The combination of extraction and chronocoulometry of a solid precipitate for teaching a novel approach of electroanalysis," *Journal of Solid State Electrochemistry*, Dec. 2023, doi: 10.1007/s10008-023-05764-8.

[50] T. Morimoto, E. Hara, and H. Katoh, “Application of chronocoulometry method for measuring Fick’s diffusion constant of thin coating layers,” *Advanced Composite Materials*, vol. 32, no. 1, pp. 21–34, Jan. 2023, doi: 10.1080/09243046.2022.2070948.

[51] E. D. Pomeroy, W. A. Maza, D. A. Steinhurst, J. C. Owrutsky, and R. A. Walker, “Electrochemical Sulfur Oxidation in Solid Oxide Fuel Cells Studied by Near Infrared Thermal Imaging and Chronocoulometry,” *J Electrochem Soc*, vol. 167, no. 16, p. 164511, Dec. 2020, doi: 10.1149/1945-7111/abcc31.

[52] J. M. Marioli and T. Kuwana$, “ELECTROCHEMICAL CHARACTERIZATION OF CARBOHYDRATE OXIDATION AT COPPER ELECTRODES,” 1992.

[53] J. Come, P.-L. Taberna, S. Hamelet, C. Masquelier, and P. Simon, “Electrochemical Kinetic Study of LiFePO4 Using Cavity Microelectrode,” *J Electrochem Soc*, vol. 158, no. 10, p. A1090, 2011, doi: 10.1149/1.3619791.

[54] N. Yu *et al.*, “Facile fabrication of low-cost and scalable graphite tape as novel current collectors for flexible supercapacitors,” *J Alloys Compd*, vol. 861, Apr. 2021, doi: 10.1016/j.jallcom.2020.158476.

[55] K. Pushnitsa, A. Kosenko, V. Chernyavsky, A. A. Pavlovskii, P. Novikov, and A. A. Popovich, “Copper-Coated Graphite Felt as Current Collector for Li-Ion Batteries,” *Coatings*, vol. 12, no. 9, Sep. 2022, doi: 10.3390/coatings12091321.

[56] V. Babaahmadi, S. E. M. Pourhosseini, O. Norouzi, and H. R. Naderi, “Designing 3D Ternary Hybrid Composites Composed of Graphene, Biochar and Manganese Dioxide as High-Performance Supercapacitor Electrodes,” *Nanomaterials*, vol. 13, no. 12, Jun. 2023, doi: 10.3390/nano13121866.

[57] V. Poltavets, M. Krawczyk, G. Maslak, O. Abraimova, and M. Jönsson-Niedziółka, “Formation of MnO2-coated ITO electrodes with high catalytic activity for enzymatic glucose detection,” *Dalton Transactions*, vol. 52, no. 38, pp. 13769–13780, Sep. 2023, doi: 10.1039/d3dt02199h.

[58] M. A. B. Siddique *et al.*, "Preparation of Manganese Oxide Nanoparticles with Enhanced Capacitive Properties Utilizing Gel Formation Method," *ACS Omega*, vol. 7, no. 51, pp. 48007–48017, Dec. 2022, doi: 10.1021/acsomega.2c05872.

[59] K. Liang, M. Zhou, and W. Hu, "Data analysis preparation and characterization of porous manganese oxide films for super capacitor by cathodic electrode position," 2015.

[60] Y. Wang and I. Zhitomirsky, "Electrophoretic deposition of manganese dioxide - Multiwalled carbon nanotube composites for electrochemical supercapacitors," *Langmuir*, vol. 25, no. 17, pp. 9684–9689, Sep. 2009, doi: 10.1021/la900937e.

[61] T. Bordjiba and D. Bélanger, "Direct Redox Deposition of Manganese Oxide on Multiscaled Carbon Nanotube/Microfiber Carbon Electrode for Electrochemical Capacitor," *J Electrochem Soc*, vol. 156, no. 5, p. A378, 2009, doi: 10.1149/1.3090012.

[62] A. Yavuz, K. Kaplan, and M. Bedir, "Metal oxides composite electrode with high areal capacitance formed by thermal oxidation of stainless steel mesh," *Journal of Solid State Electrochemistry*, vol. 26, no. 6–7, pp. 1333–1347, Jul. 2022, doi: 10.1007/s10008-022-05160-8.

CURRICULUM VITAE

Name Surname **Bilal MANSOUR**

EDUCATION

2024 **M.Sc. in Materials Science and Engineering**
Gaziantep University, Department of Materials Science and Engineering.
Thesis Title: Manganese Based Electrodes in Alkaline and Neutral Electrolytes for Flexible Energy Storage Devices.

2014 **B.Sc. in Mechanical Engineering**
Aleppo University, Faculty of Mechanical Engineering,
Department of Material Science and Engineering
Dissertation project: Copper Iron Alloys

PROFESSIONAL EXPERIENCE

2023 up to date **Internal Auditor – Bonyan Organization**
Responsible for evaluating and improving the effectiveness of governance, risk management, and control processes. Ensures compliance with laws, regulations, and organization's policies; identifies any areas of potential improvement.

2019 to 2023 **Quality Assurance Manager/Co-Founder– Business Insight**
Oversees the development and implementation of quality assurance and control systems. As a co-founder, also involved in strategic planning and ensuring the business's services or products meet consistent standards.

2016 to 2021 **MEAL Manager– Bonyan Organization (Contract)**
Manages the Monitoring, Evaluation, Accountability, and Learning (MEAL) systems to track project performance and outcomes. Develops MEAL frameworks, ensuring that lessons learned are integrated into project planning and decision-making.

ADDITIONAL INFORMATION

Membership Member of **Institution of Internal Auditors-Türkiye Chapter**